# NACA

RESEARCH MEMORANDUM

EFFECTS OF HORIZONTAL-TAIL POSITION, AREA,

AND ASPECT RATIO ON LOW-SPEED STATIC LONGITUDINAL STABILITY

AND CONTROL CHARACTERISTICS OF A 60° TRIANGULAR-WING MODEL

HAVING VARIOUS TRIANGULAR-ALL-

MOVABLE HORIZONTAL TAILS

By Byron M. Jaquet

Langley Aeronautical Laboratory
Langley Field, Va.

NATIONAL ADVISORY COMMITTEE
FOR AERONAUTICS

WASHINGTON

December 14, 1951
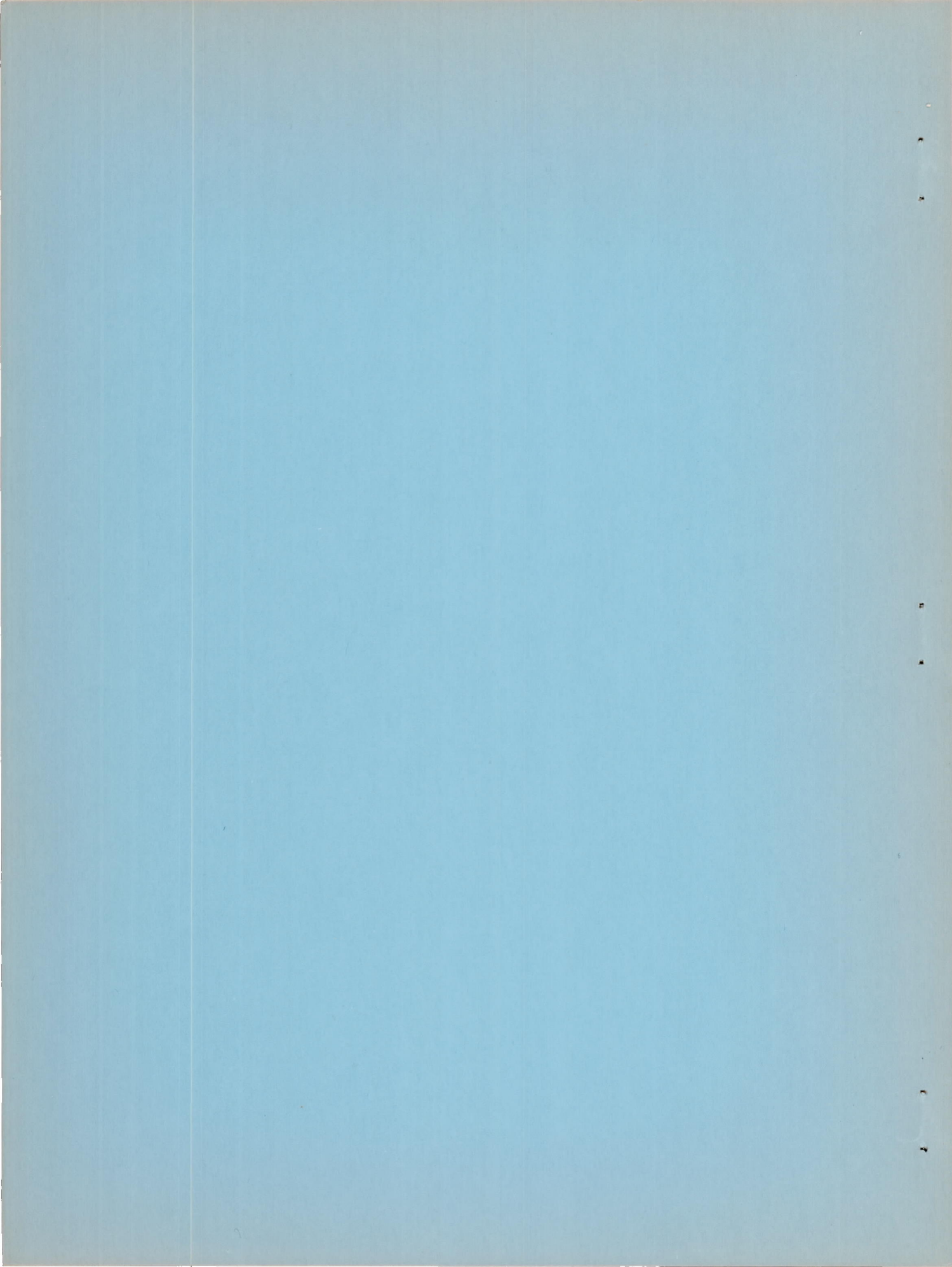
NATIONAL ADVISORY COMMITTEE FOR AERONAUTICS

RESEARCH MEMORANDUM

EFFECTS OF HORIZONTAL-TAIL POSITION, AREA,

AND ASPECT RATIO ON LOW-SPEED STATIC LONGITUDINAL STABILITY

AND CONTROL CHARACTERISTICS OF A 60° TRIANGULAR-WING MODEL

HAVING VARIOUS TRIANGULAR-ALL-

MOVABLE HORIZONTAL TAILS

By Byron M. Jaquet

SUMMARY

A low-speed investigation was made in the Langley stability tunnel to determine the static longitudinal stability and control character-istics of a 60° triangular-wing model having various triangular-all-movable horizontal tails. An all-movable tail of 10 percent of the wing area and aspect ratio 2.31 was investigated in 17 tail positions which included positions above, below, and to the rear of the assumed center of gravity. All-movable tails of 5 and 15 percent of the wing area (aspect ratio 2.31) and an all-movable tail of aspect ratio 1.07 (5-percent-area) were investigated at one tail position.

At high angles of attack, large increases in the rate of change of effective downwash angle with angle of attack caused large decreases in the static longitudinal stability of most configurations. The high-forward and low-rearward tail positions were least affected by changes in downwash angle with angle of attack and, consequently, these positions had the most favorable stability characteristics. For one position, an increase in tail area from 5 to 15 percent of the wing area produced an increase in static longitudinal stability at low lift coefficients and instability (associated with large increases in the rate of change of downwash angle with angle of attack) at high lift coefficients.

An increase in tail length for a given tail height produced an increase in pitching-moment effectiveness which was approximately directly proportional to the tail length but had insignificant effects on the change in lift with control deflection. An increase in tail height produced a small increase in pitching-moment effectiveness.

All-movable-triangular tails had about 20 percent less pitching-moment
effectiveness (which was essentially constant up to maximum lift) than
constant-chord flap controls of about the same area and were about twice
as effective as half-delta tip controls. The all-movable tails produced
less lift per degree of control deflection (which also was essentially
constant up to maximum lift) than the constant-chord flap controls or
half-delta tip controls.

The tail position for maximum pitching-moment effectiveness was
high and rearward in contrast to a low-rearward position for the most
desirable static longitudinal stability.

INTRODUCTION

Wings of triangular plan form appear, in many respects, to be
structurally and aerodynamically suitable for high-speed airplanes;
however, adequate longitudinal control is difficult to obtain for these
airplanes with manually operated controls. For example, constant-chord
flap controls have good effectiveness at low speeds, but inherently
have undesirably high hinge moments (references 1 and 2), and half-delta
tip controls, which permit a wide choice of hinge location for aero-
dynamic balance, have low control effectiveness at low speeds (refer-
ence 3). In another case, a canard was found to be virtually ineffective
as a fixed trimming device at high lift coefficients in a low-speed
investigation of a canard triangular-wing arrangement (reference 4). In
a low-speed investigation of a 45° triangular-wing model conducted in
Great Britain[1] by Lock, Pass, and Meikler, some promise has been indicated
for all-movable tails located behind the center of gravity although some
instability was encountered near the stall. An all-movable tail, in
addition to providing longitudinal control, should overcome some of the
other difficulties encountered with semitailless airplanes. The hori-
zontal tail would provide additional damping in pitch, which is low for
triangular wings (reference 5), and perhaps eliminate the possibility
of tumbling (a continuous pitching rotation about the lateral axis) which
is also associated with semitailless airplanes. In addition, the center-
of-gravity travel would not be as severely restricted for an airplane
with horizontal tail.

Inasmuch as triangular-wing airplanes generally have stable
pitching-moment characteristics through the lift-coefficient range, a
horizontal tail would be expected to be necessary only as a control and
not as a stabilizer. In the present investigation (which is a part of
a research program being conducted in the Langley stability tunnel to

---

[1]Not generally available.

determine the suitability of various types of controls for triangular wings), addition of a horizontal tail, however, resulted in serious instability for some tail positions. It was, therefore, desirable to determine an optimum, or nearly optimum, tail position with regard to static stability as well as control effectiveness. Thus, the effects of tail length, height, area, and aspect ratio on the low-speed static longitudinal stability and control characteristics of a 60° triangular wing model having various all-movable triangular tails located behind the center of gravity of the model were studied in this investigation. The results for all-movable tails were compared with results for constant-chord flap controls and half-delta tip controls of the same area.

SYMBOLS

The data presented herein are in the form of standard NACA symbols and coefficients of forces and moments and are referred to the stability system of axes with the origin at the projection of the quarter-chord point of the mean aerodynamic chord on the plane of symmetry unless otherwise specified. The positive direction of forces, moments, and angular displacements is indicated in figure 1. The coefficients and symbols used herein are defined as follows:

C_L lift coefficient $\left(\dfrac{L}{qS}\right)$

C_m pitching-moment coefficient $\left(\dfrac{M}{qS\bar{c}}\right)$

L lift, pounds

M pitching moment, foot pounds

A aspect ratio $\left(b^2/S\right)$

b span, feet

S wing area, square feet

S_H horizontal-tail area, square feet

c local chord parallel to plane of symmetry, feet

$\bar{c}$ mean aerodynamic chord, feet $\left(\dfrac{2}{S}\displaystyle\int_{0}^{b/2} c^2\,dy\right)$

c_r root chord, feet

y spanwise distance measured from and perpendicular to plane of symmetry, feet

q free-stream dynamic pressure, pounds per square foot $\left(\dfrac{\rho V^2}{2}\right)$

q_t dynamic pressure at tail, pounds per square foot

V free-stream velocity, feet per second

ρ density of air, slugs per cubic foot

l tail length, feet (distance between quarter-chord point of wing mean aerodynamic chord and quarter-chord point of tail mean aerodynamic chord measured along the fuselage center line)

z tail height (height of tail above or below the wing-chord plane), feet

α angle of attack of wing-chord plane, degrees

i_t angle of incidence of tail with respect to wing-chord plane, degrees

Λ_{LE} angle of sweepback of leading edge, degrees

ϵ_e effective downwash angle, degrees

$\left(\dfrac{q_t}{q}\right)_e$ effective dynamic pressure ratio $\left(\dfrac{C_{m_{i_t}}}{\left(C_{m_{i_t}}\right)_o}\right)$

$$C_{L_{i_t}} = \frac{\partial C_L}{\partial i_t}$$

$$C_{m_{i_t}} = \frac{\partial C_m}{\partial i_t}$$

$$\left(C_{m_{i_t}}\right)_o = \left(\frac{\partial C_m}{\partial i_t}\right)_{C_L = 0}$$

$$C_{L_\alpha} = \frac{\partial C_L}{\partial \alpha}$$

$$C_{m_{C_L}} = \frac{\partial C_m}{\partial C_L}$$

H   horizontal tail

Subscripts:

1   horizontal tail 1

2   horizontal tail 2

3   horizontal tail 3

4   horizontal tail 4

APPARATUS, MODEL, AND TESTS

The present investigation was conducted in the 6- by 6-foot test section of the Langley stability tunnel. The model was mounted on a single-strut support with the pivot point at the quarter chord of the mean aerodynamic chord. The strut was attached to a six-component balance system.

The model consisted of a mahogany wing-fuselage combination and four mahogany horizontal tails which were tested individually. The wing had an aspect ratio of 2.31, $\Lambda_{LE} = 60^\circ$, and modified NACA $65_{(06)}$-006.5 airfoil sections parallel to the plane of symmetry. The fuselage had a circular cross section and a fineness ratio of 7.38. Additional details of the fuselage may be obtained from reference 6. Three of the horizontal tails had the same plan form and thickness ratio as the wing but had areas of 5, 10, and 15 percent of the wing area. An additional tail of aspect ratio 1.07, $\Lambda_{LE} = 75^\circ$, and an area of 5 percent of the wing area was used for a few tests. The tails were supported by $\frac{1}{4}$- by 2-inch steel support struts (one strut was used for each tail height) mounted on a $\frac{3}{4}$- by $\frac{1}{2}$- by 45-inch steel bar, the lower surface of which was parallel to but 1.5 inches above the fuselage center line. Pertinent model details and tail locations are shown in figure 2 and details of the horizontal tails are shown in figure 3. Tails 1, 3, and 4 were

tested at one position only $\left(\dfrac{z}{\bar{c}} = 0.50, \quad \dfrac{l}{\bar{c}} = 1.25\right)$. A photograph of one model configuration is presented as figure 4.

The tests consisted of measurement of lift and pitching moment through an angle-of-attack range of $-4°$ to $36°$ for several angles of incidence of the tails. All tests were conducted at a dynamic pressure of 39.7 pounds per square foot, a Mach number of 0.17, and a Reynolds number of 2.06×10^6.

CORRECTIONS

Approximate jet-boundary corrections (reference 7), based on unswept-wing concepts, have been applied to the angle of attack. Complete-model (tail on) pitching moments have been corrected for jet-boundary effects by the methods of reference 8 and the dynamic pressure was corrected for the effects of blockage by the methods of reference 9. The data have not been corrected for the effects of the support strut.

RESULTS AND DISCUSSION

Presentation of Results

Table I is presented as an index to the figures to aid in the location of specific data from the large number of figures.

The control effectiveness parameters $C_{L_{i_t}}$ and $C_{m_{i_t}}$ represent slopes of faired curves measured near zero tail incidence for a constant angle of attack. The slopes, however, were generally linear between $i_t = 10°$ and $i_t = -20°$.

The effective downwash angles were determined at a given angle of attack by the sum of the angle of attack and the angle of incidence of the tail which produced the zero pitching-moment contirubution of the tail. The effective dynamic-pressure ratios were determined from the pitching-moment data in the following manner:

$$\left(\frac{q_t}{q}\right)_e = \frac{C_{m_{i_t}}}{\left(C_{m_{i_t}}\right)_o}$$

where $\left(C_{m_{i_t}}\right)_0$ is the value at $C_L = 0$ for any tail position and $C_{m_{i_t}}$ is the value at any lift coefficient for the same tail position. This assumption always gives a value of $\left(q_t/q\right)_e$ of 1.0 at $C_L = 0$ and is believed to be accurate within 2 or 3 percent.

The basic data $\left(C_m \text{ and } \alpha \text{ against } C_L\right)$ of figures 5 to 25 will be given only brief consideration inasmuch as the analysis of the present paper is concerned with figures 26 to 45. The lift-curve slope and C_m/C_L at $C_L = 0$ of the wing and wing-fuselage combination are in good agreement with previous investigations (reference 6). The wing maximum lift coefficient is also about the same as that of reference 6; however, the wing-fuselage maximum lift coefficient is about 10 percent lower than that obtained previously. The lift and pitching-moment characteristics of the wing-fuselage and horizontal-tail configurations are presented in figures 6 to 25. The static longitudinal stability at trim decreases with an increase in trim lift coefficient for tail positions above the wing-chord plane (figs. 6 to 20 and figs. 23 to 25) and increases with an increase in trim lift coefficient for tail positions below the wing-chord plane (figs. 21 and 22).

Longitudinal Stability

Effect of tail length and height.- For convenience the basic data at $i_t = 0°$ of figures 6 to 22 have been replotted in figures 26 and 27.

From figures 26 and 27 it can be seen that the wing-fuselage combination is stable through the lift-coefficient range for the test center-of-gravity position. The data of figures 26 and 27 also indicate that addition of the horizontal tail (10 percent of the wing area) to the wing-fuselage combination produces an increase in longitudinal stability at low lift coefficients. The stability increases with an increase in tail length or height.

Generally, as the lift coefficient is increased to some moderate value, a decrease occurs in stability. With a further increase in lift coefficient, there is either an increase in stability or a further decrease depending on the tail length and height. The effects of tail length and height on the changes in stability with lift coefficient can probably be seen best from the data of figures 28 and 29 which were obtained by recomputing the data of figures 26 and 27 about a different center-of-gravity position for each configuration to give a static margin at $C_L = 0$ of 10 percent of the mean aerodynamic chord. The position of the center of gravity for each configuration for which data

are presented with $C_{m_{C_L}} = -0.10$ in figures 28 and 29 is as follows:

$z/\bar{c}$	$l/\bar{c}$	Center of gravity (percent $\bar{c}$)
0.25	0.75 1.00 1.25 1.50 2.00	29.6 30.5 31.6 33.1 34.7
0.50	0.75 1.00 1.25 1.50 2.00	30.7 32.2 33.5 35.5 38.0
0.75	0.75 1.00 1.25 1.50 2.00	31.4 32.9 35.1 36.9 39.9
-0.06	1.50 2.00	31.6 32.9

The center of gravity of the wing-fuselage combination is at $0.275\bar{c}$.

The data of figure 28 indicate that at high lift coefficients an increase in stability with an increase in tail length is obtained at a tail height of $\frac{z}{c} = 0.25$. At tail heights greater than $\frac{z}{c} = 0.25$, the stability decreases with an increase in tail length and, for high-rearward positions, severe instability occurs. The configurations with the high-forward and low-rearward tail positions exhibit the least change in static longitudinal stability through the lift-coefficient range and only tail positions below the wing-chord plane (fig. 29) provide stability equal to, or better than, that for the wing-fuselage combination. The small positive increment in pitching moment present at low lift coefficients with the addition of a horizontal tail (figs. 28 and 29) is believed to be caused by flow induced by the fuselage and this increment appears to decrease with an increase in tail length or height.

The effect of the horizontal-tail position on the longitudinal stability from $C_L = 0$ to $C_L = 0.8$ is summarized in figure 30. The regions of least change in $\partial C_m / \partial C_L$ are located in the high-forward or low-rearward positions. As mentioned previously only tail positions below the wing-chord plane produce stability equal to or greater than that for the wing-fuselage combination through the lift-coefficient range and thus the change in $\partial C_m / \partial C_L$ noted for these positions is stabilizing.

The changes in stability which occur, for tail-on configurations, as the lift coefficient is increased, can be associated primarily with large increases in downwash angle with angle of attack and to some extent with the change in the ratio $\left(q_t/q\right)_e$ with angle of attack (figs. 31 to 38). The effects of tail length and height on the variation of the effective downwash angle with angle of attack are shown in figures 31 to 35. The rate of change of effective downwash with angle of attack $\partial \epsilon_e / \partial \alpha$ varies considerably with angle of attack. The values of $\partial \epsilon_e / \partial \alpha$ at $\alpha = 0^\circ$ are presented in figure 36 for the tail positions investigated. These values of $\partial \epsilon_e / \partial \alpha$ are always less than 1 and decrease with an increase in tail length or height. Therefore, as mentioned previously, addition of a tail always results in an increase in stability at low lift coefficients (figs. 26 and 27). As the angle of attack is increased however, the value of $\partial \epsilon_e / \partial \alpha$ increases rapidly and reaches a value of 2.0 for some configurations. The configurations for which large decreases in stability occur with increases in lift coefficient and which become unstable are those for which $\partial \epsilon_e / \partial \alpha$ becomes sufficiently greater than 1.0 to overcome the inherent stability of the wing-fuselage combination. For tail positions below the wing-chord plane the effective downwash angles at high angles of attack were much less than that for most of the other configurations. The values of $\partial \epsilon_e / \partial \alpha$ were near zero or even negative and, as mentioned previously, these positions provided greater stability than the wing-fuselage combination in the high lift-coefficient range. It should be noted that the values of downwash angle shown at $\alpha = 0^\circ$ for a tail height of $\frac{z}{c} = 0.25$ (fig. 31) are probably caused by flow over the end of the fuselage.

The effects of tail length and height on the variation of $\left(q_t/q\right)_e$ with angle of attack are presented for several model configurations in figures 37 and 38. The largest changes in $\left(q_t/q\right)_e$ occur at high angles of attack. A loss in $\left(q_t/q\right)_e$ in the high angle-of-attack region is beneficial for some tail lengths, especially for $\frac{z}{c} = 0.75$, since it tends to reduce the instability (fig. 28) where $\partial \epsilon_e / \partial \alpha$

(fig. 33) is large. Conversely, an increase in $(q_t/q)_e$ at moderate and high angles of attack can magnify the instability caused by high values of $\partial\epsilon_e/\partial\alpha$. See, for example, figures 29, 34, and 38 for $\frac{z}{c} = 0.50$ and $\frac{l}{c} = 1.50$ for which $(q_t/q)_e$ increases at about 16° angle of attack and $\partial\epsilon_e/\partial\alpha$, already greater than that for the other tail positions, is effectively increased again by the increase in $(q_t/q)_e$ greater instability thereby being caused.

Effect of tail area and aspect ratio.- The effects of tail area and aspect ratio on the static longitudinal stability of the model for one tail position $\left(\frac{z}{c} = 0.50 \quad \text{and} \quad \frac{l}{c} = 1.25\right)$ are shown in figure 39. An increase in tail area from 5 to 15 percent of the wing area causes an increase in stability up to about $C_L = 0.4$; whereas, at lift coefficients between 0.4 and 0.7, the stability does not change appreciably when the tail area is increased (fig. 39(a)). At high lift coefficients, near maximum lift, instability results for the 10- and 15-percent-area tails. A decrease in the aspect ratio of the 5-percent-area tail from 2.31 to 1.07 has little effect on stability through the lift-coefficient range. It should be remembered that, for triangular plan forms, a decrease in aspect ratio is accompanied by an increase in sweep angle and thus the effects of aspect ratio and sweep are inseparable.

In order to illustrate the effects of tail area and aspect ratio on the changes in stability with lift coefficient, the data are compared on the basis of equal static margin at $C_L = 0$. The position of the center of gravity for each configuration for which data are presented with $C_{m_{C_L}} = -0.10$ in figure 39(b) is as follows:

H	Center of gravity (percent $\overline{c}$)
1	30.6
2	33.5
3	36.5
4	29.6

The center of gravity of the wing-fuselage combination is at $0.275\overline{c}$. The large changes in stability which occur for the 10- and 15-percent-area tails are readily discernible from figure 39(b). A reduction in tail aspect ratio from 2.31 to 1.07 has relatively small effect on stability, the $A = 1.07$ tail providing an increase in stability for only a small range of lift coefficients near the stall.

As mentioned previously, the changes to stability with angle of attack can be associated with changes in downwash angle with angle of attack and to some extent with changes in $(q_t/q)_e$ with angle of attack. Values of $\partial\epsilon_e/\partial\alpha$ and $(q_t/q)_e$ are presented in figures 40 to 42. Large increases in $\partial\epsilon_e/\partial\alpha$ (fig. 40) at high angles of attack cause instability for tails 2 and 3 at this tail position. The span of these tails is believed to be sufficiently large to be affected by the separation vortex which is swept toward the plane of symmetry as the angle of attack is increased. Tails 1 and 4 do not extend outboard from the plane of symmetry a large enough distance to be greatly affected by the vortex and, hence, do not produce instability at high lift coefficients (fig. 39).

Control Effectiveness

The control effectiveness data for all model configurations of figures 43 to 45 are presented on a basis of equal static longitudinal stability at $C_L = 0$ $\left(C_{m_{C_L}} = -0.10\right)$ and thus the data are directly indicative of the effects of tail length, height, area, and aspect ratio on the control effectiveness parameter $C_{m_{i_t}}$. The position of the center of gravity for each configuration of figures 43 and 44 may be obtained from the table in the section entitled "Longitudinal Stability." The centers of gravity for the configurations of figure 45 are presented subsequently in this section.

Effect of tail length and height.- An increase in lift coefficient produces only small changes in the values of $C_{L_{i_t}}$ and $C_{m_{i_t}}$ up to about maximum lift coefficient for each model configuration (fig. 43). The best tail position with regard to static longitudinal stability through the lift-coefficient range was $\frac{z}{c} = -0.06$ and $\frac{l}{c} = 2.00$; whereas the maximum pitching-moment effectiveness through the lift-coefficient range was obtained at $\frac{z}{c} = 0.50$ and $\frac{l}{c} = 2.00$. The pitching-moment effectiveness data for these two positions is presented in figure 43(e). At low lift coefficients, the position for maximum $C_{m_{i_t}}$ provides a value of $C_{m_{i_t}}$ of about 10 percent greater than the value of $C_{m_{i_t}}$ for the position of best stability; whereas at high lift coefficients the difference amounts to about 23 percent. The position for maximum $C_{m_{i_t}}$ is one, however, where severe instability occurs at

moderate lift coefficients. (See fig. 29.) A tail position of $\frac{z}{\bar{c}} = 0.25$ and $\frac{l}{\bar{c}} = 2.00$ has satisfactory static longitudinal stability (fig. 29) and, except for high lift coefficients, has about the same pitching-moment effectiveness as the tail position $\frac{z}{\bar{c}} = 0.50$ and $\frac{l}{\bar{c}} = 2.00$. Of the positions investigated, a low-forward position had the lowest control effectiveness (fig. 44(a)).

The effects of tail length and tail height on the values of $C_{L_{i_t}}$ and $C_{m_{i_t}}$ at $C_L = 0$ are summarized in figure 44. Changes in tail length or height generally produce only small changes in the value of $C_{L_{i_t}}$. The value of $C_{m_{i_t}}$ increases with an increase in tail length in about direct proportion to the tail length and increases slightly with an increase in tail height. Trends similar to those of the present paper were indicated in the previously mentioned British investigation of a $45°$ triangular-wing model having a separate-all-movable tail. In that investigation, however, only two tail lengths were investigated.

<u>Effect of tail area and aspect ratio</u>.- The data presented in figure 45 are also for $C_{m_{C_L}} = -0.10$ at $C_L = 0$ and the centers of gravity for the configurations are as follows:

Configuration	H	Center of gravity (percent $\bar{c}$)
All-movable tails	1 2 3 4	30.6 33.5 36.5 29.6
Constant-chord flaps Tip controls		27.4 29.2

An increase in tail area from 5 to 15 percent of the wing area causes a proportional increase in $C_{L_{i_t}}$ and $C_{m_{i_t}}$ (fig. 45(a)) which are about constant up to maximum lift coefficient. Reducing the aspect ratio of the 5-percent-area tail from 2.31 to 1.07 causes a decrease in $C_{L_{i_t}}$ and $C_{m_{i_t}}$ which is constant up to maximum lift coefficient.

A comparison of the effectiveness at $C_L = 0$ of the all-movable tails of the present investigation with the constant-chord flaps of reference 1 and the tip controls of reference 3 is presented in figure 45(b) for $C_{m_{C_L}} = -0.10$. Each of the controls was tested on a wing of identical geometry. The all-movable tails produce a slightly smaller change in lift with control deflection $C_{L_{i_t}}$ than the tip controls (which is desirable) and, as would be expected, a much smaller change in lift with control deflection than the constant-chord flaps. From a standpoint of pitching-moment effectiveness $C_{m_{i_t}}$ the all-movable tails are about twice as effective as the tip controls and are about 20 percent less effective than the constant-chord flaps.

CONCLUSIONS

A low-speed investigation of the static longitudinal stability and control characteristics of a 60° triangular-wing model having various all-movable horizontal tails has indicated the following conclusions:

1. At high angles of attack large increases in the rate of change of effective downwash angle with angle of attack caused large decreases in the static longitudinal stability of most of the configurations. The high-forward and low-rearward tail positions were least affected by changes in downwash angle with angle of attack and, consequently, these positions had the most favorable stability characteristics.

2. For one position, an increase in tail area from 5 to 15 percent of the wing area produced an increase in static longitudinal stability at low lift coefficients and instability (associated with large increases in the rate of change of downwash angle with angle of attack) at high lift coefficients.

3. An increase in tail length for a given tail height produced an increase in pitching-moment effectiveness which was approximately directly proportional to the tail length and had insignificant effects on the change in lift with control deflection. An increase in tail height produced a small increase in pitching-moment effectiveness.

4. All-movable-triangular tails had about 20 percent less pitching-moment effectiveness (which was essentially constant up to maximum lift) than constant-chord flap controls of about the same area and were about twice as effective as half-delta tip controls. The all-movable tails produced less lift per degree of control deflection (which also was

essentially constant up to maximum lift) than the constant-chord flap
controls or half-delta tip controls.

5. The tail position for maximum pitching-moment effectiveness was
high and rearward in contrast to a low-rearward position for the most
desirable static longitudinal stability.

Langley Aeronautical Laboratory
    National Advisory Committee for Aeronautics
        Langley Field, Va.

REFERENCES

1. Wolhart, Walter D., and Michael, William H., Jr.: Wind-Tunnel Investigation of the Low-Speed Longitudinal and Lateral Control Characteristics of a Triangular-Wing Model of Aspect Ratio 2.31 Having Constant-Chord Control Surfaces. NACA RM L50G17, 1950.

2. Stephenson, Jack D., and Ameudo, Arthur R.: Tests of a Triangular Wing of Aspect Ratio 2 in the Ames 12-Foot Pressure Wind Tunnel. II - The Effectiveness and Hinge Moments of a Constant-Chord Plain Flap. NACA RM A8E03, 1948.

3. Jaquet, Byron M., Queijo, M. J., and Lichtenstein, Jacob H.: Low-Speed Static Longitudinal Stability and Control Characteristics of a 60° Triangular-Wing Model Having Half-Delta Tip Controls. NACA RM L51D20a, 1951.

4. Bates, William R.: Low-Speed Static Longitudinal Stability Characteristics of a Canard Model Having a 60° Triangular Wing and Horizontal Tail. NACA RM L9H17, 1949.

5. Goodman, Alex, and Jaquet, Byron M.: Low-Speed Pitching Derivatives of Low-Aspect-Ratio Wings of Triangular and Modified Triangular Plan Forms. NACA RM L50C02, 1950.

6. Jaquet, Byron M., and Brewer, Jack D.: Effects of Various Outboard and Central Fins on Low-Speed Static-Stability and Rolling Characteristics of a Triangular-Wing Model. NACA RM L9E18, 1949.

7. Silverstein, Abe, and White, James A.: Wind-Tunnel Interference with Particular Reference to Off-Center Positions of the Wing and to the Downwash at the Tail. NACA Rep. 547, 1936.

8. Gillis, Clarence L., Polhamus, Edward C., and Gray, Joseph L., Jr.: Charts for Determining Jet-Boundary Corrections For Complete Models in 7- by 10-Foot Closed Rectangular Wind Tunnels. NACA ARR L5G31, 1945.

9. Herriot, John G.: Blockage Corrections for Three-Dimensional-Flow Closed-Throat Wind Tunnels, With Consideration of the Effect of Compressibility. NACA Rep. 995, 1950. (Formerly NACA RM A7B28.)

TABLE I.- INDEX TO FIGURES

Figure 1.- Stability system of axes. Arrows indicate positive direction
of forces, moments, and angular displacements.
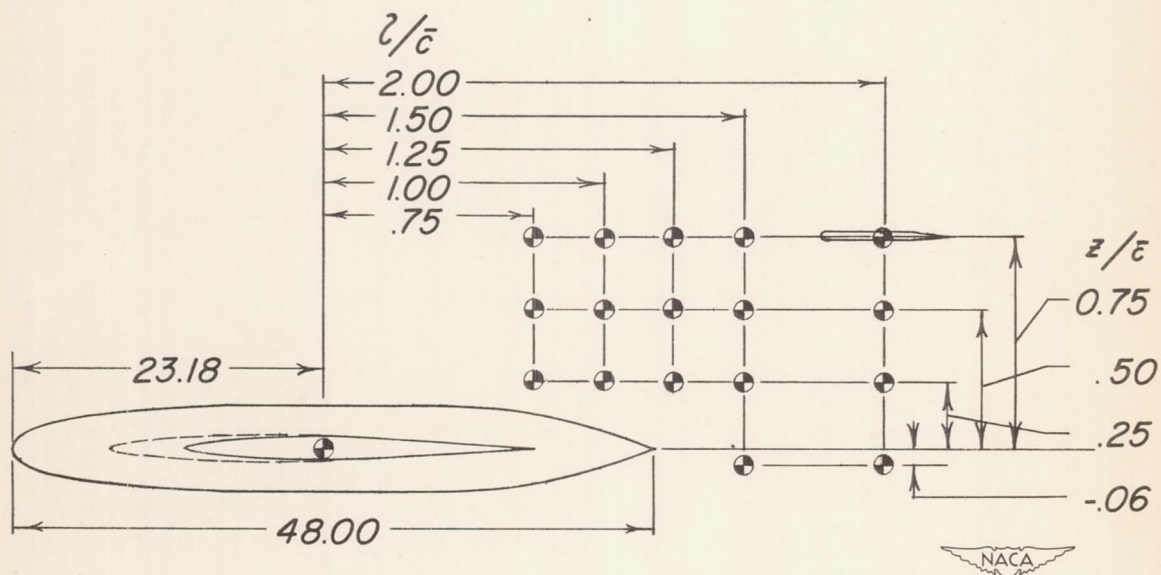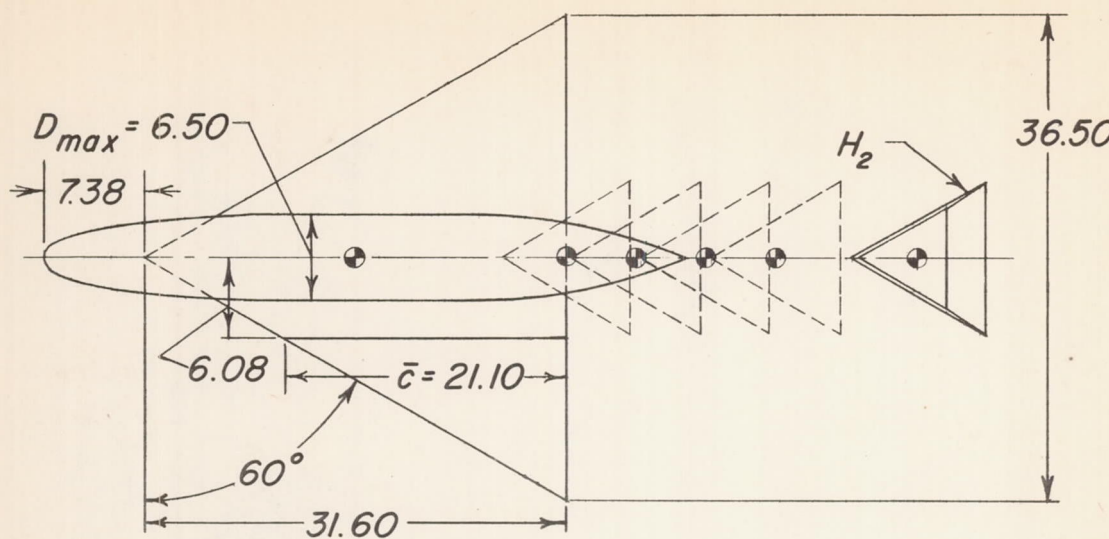
Figure 2.- Pertinent details of model. Aspect ratio of wing 2.31, area of
wing 576 square inches, airfoil section of wing NACA 65$_{(06)}$-006.5. All
dimensions are in inches.
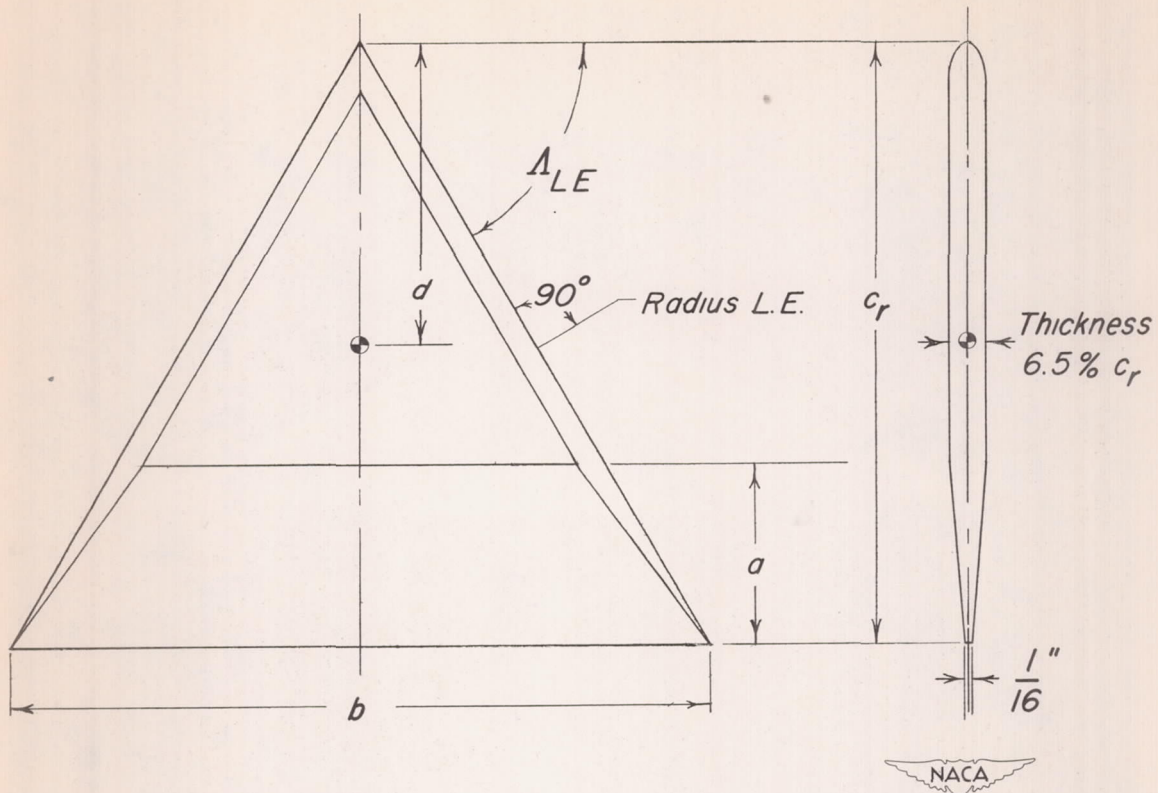
H	A	Λ_{LE} (deg)	S_H/S	a (in)	b (in)	c_r (in)	d (in)
1	2.31	60	0.05	2.12	8.16	7.06	3.53
2	2.31	60	.10	3.00	11.53	10.00	5.00
3	2.31	60	.15	3.66	14.14	12.20	6.10
4	1.07	75	.05	3.11	5.56	10.38	5.19

Figure 3.- Pertinent details of horizontal tails.
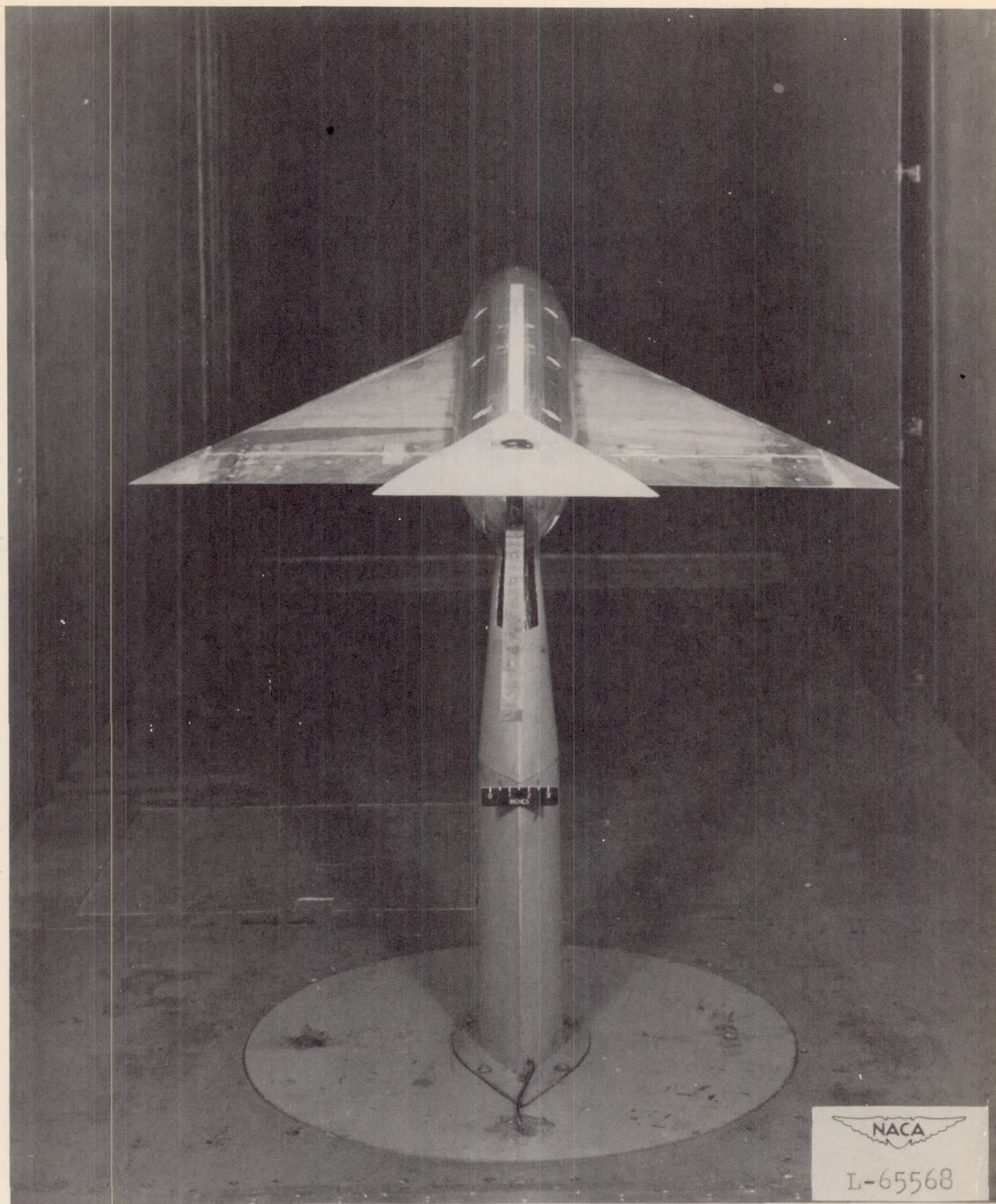
Figure 4.- Triangular-wing model mounted in Langley stability tunnel.

$$H_2; \quad \frac{z}{c} = 0.25; \quad \frac{l}{c} = 1.25.$$
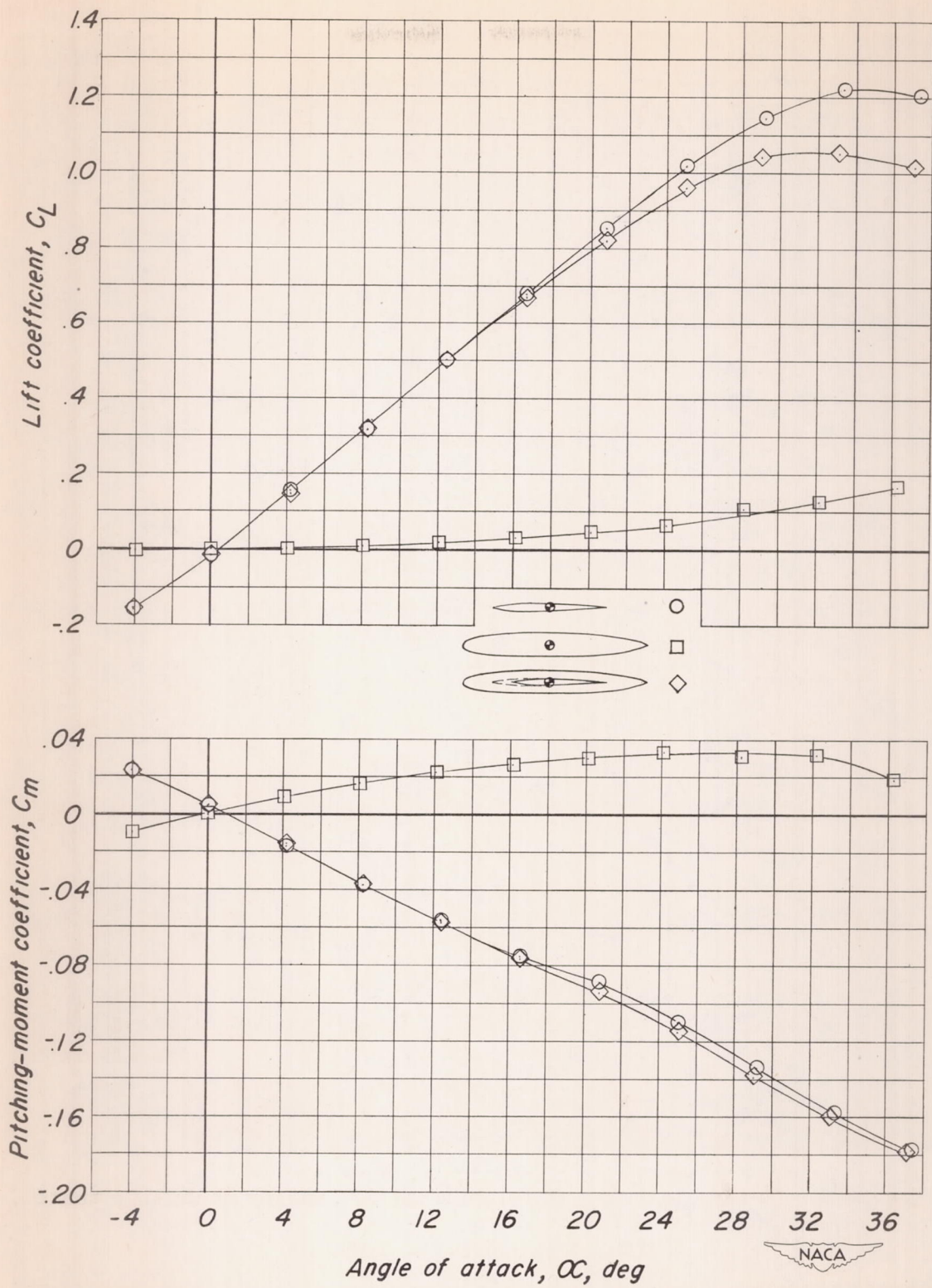
Figure 5.- Lift and pitching-moment characteristics of model components.

Figure 6.- Longitudinal stability and control characteristics of a
60° triangular-wing model having a triangular all-movable tail. H_2.
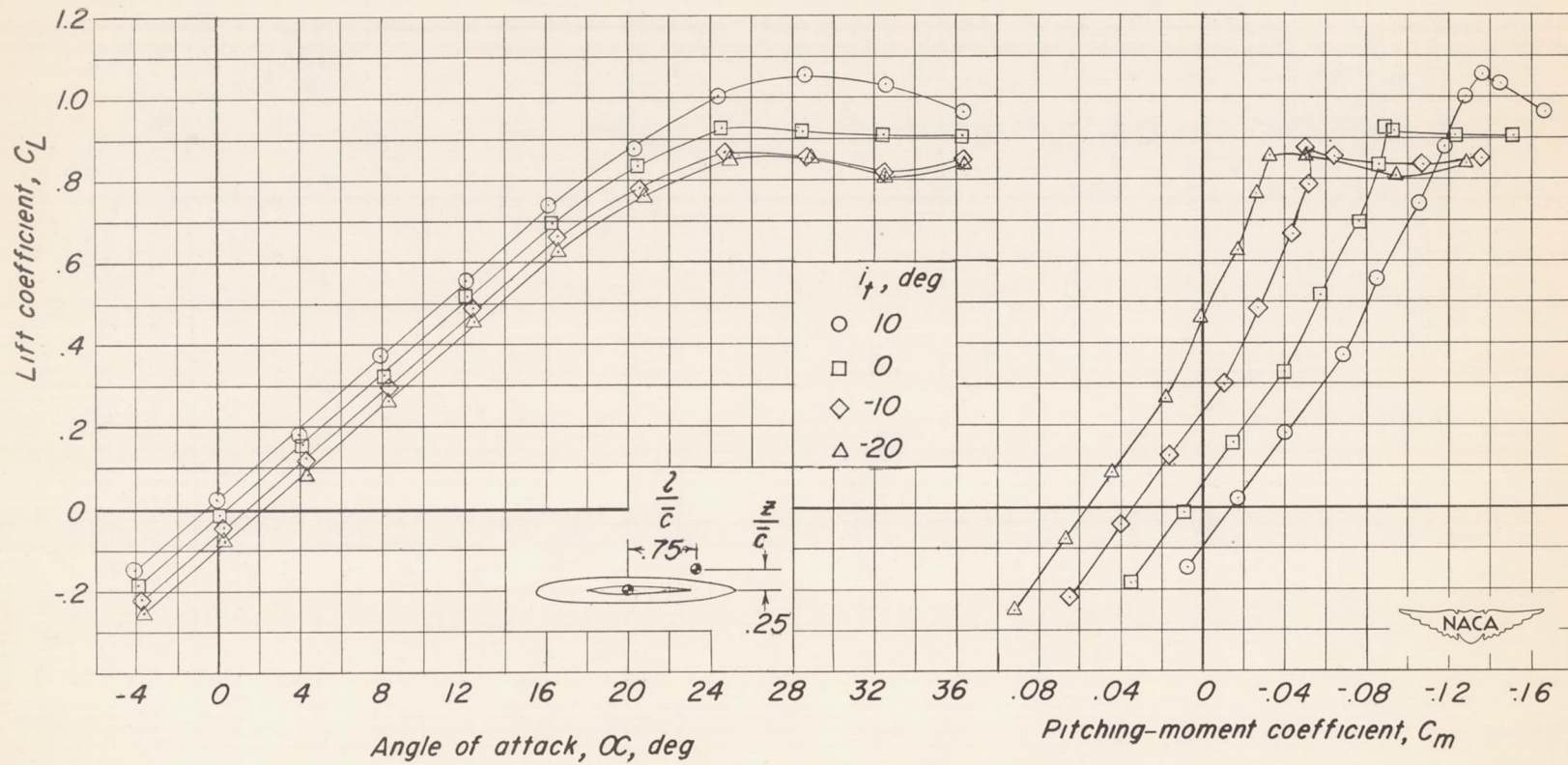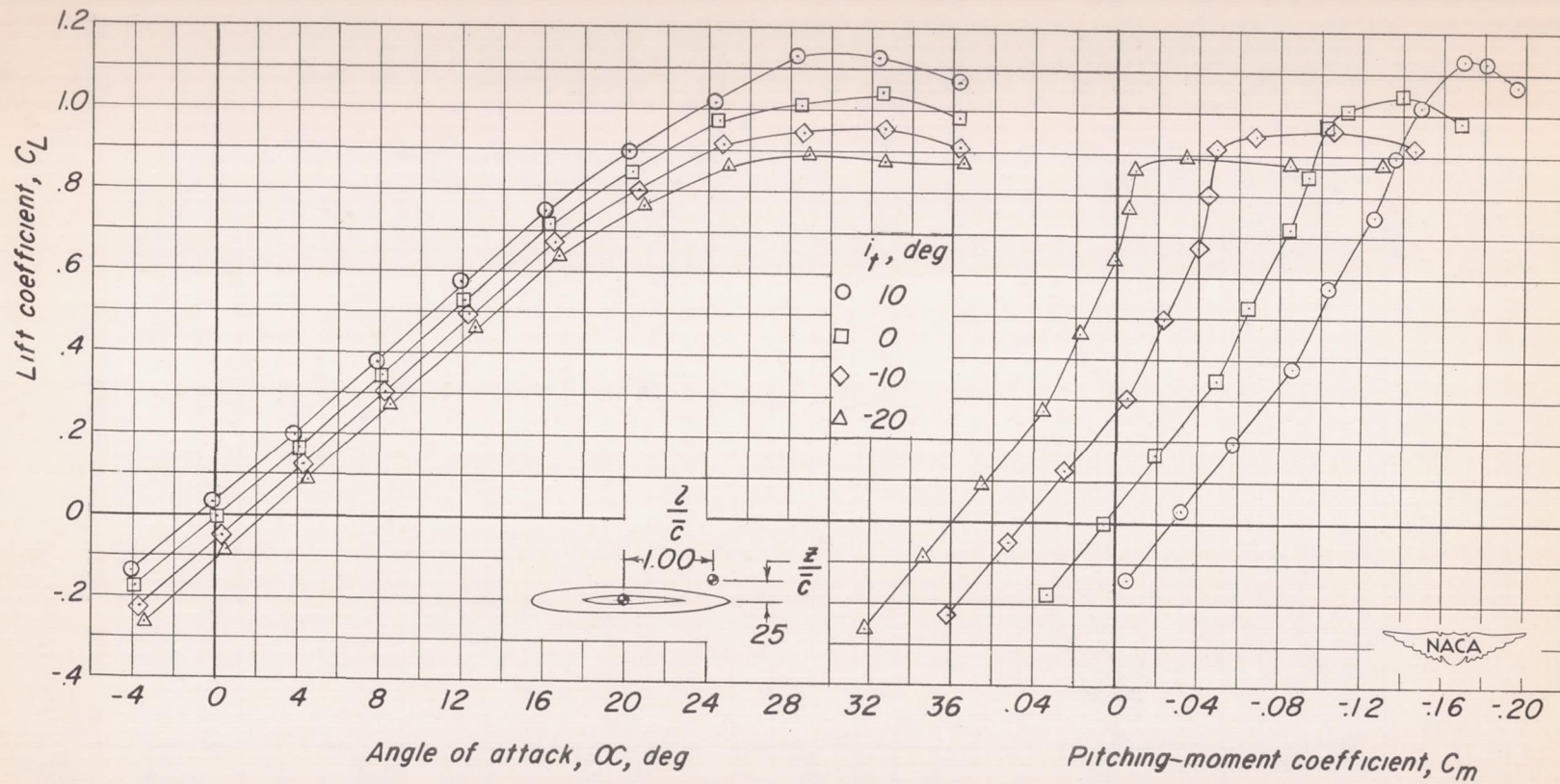
Figure 7.- Longitudinal stability and control characteristics of a
60° triangular-wing model having a triangular all-movable tail. H_2.
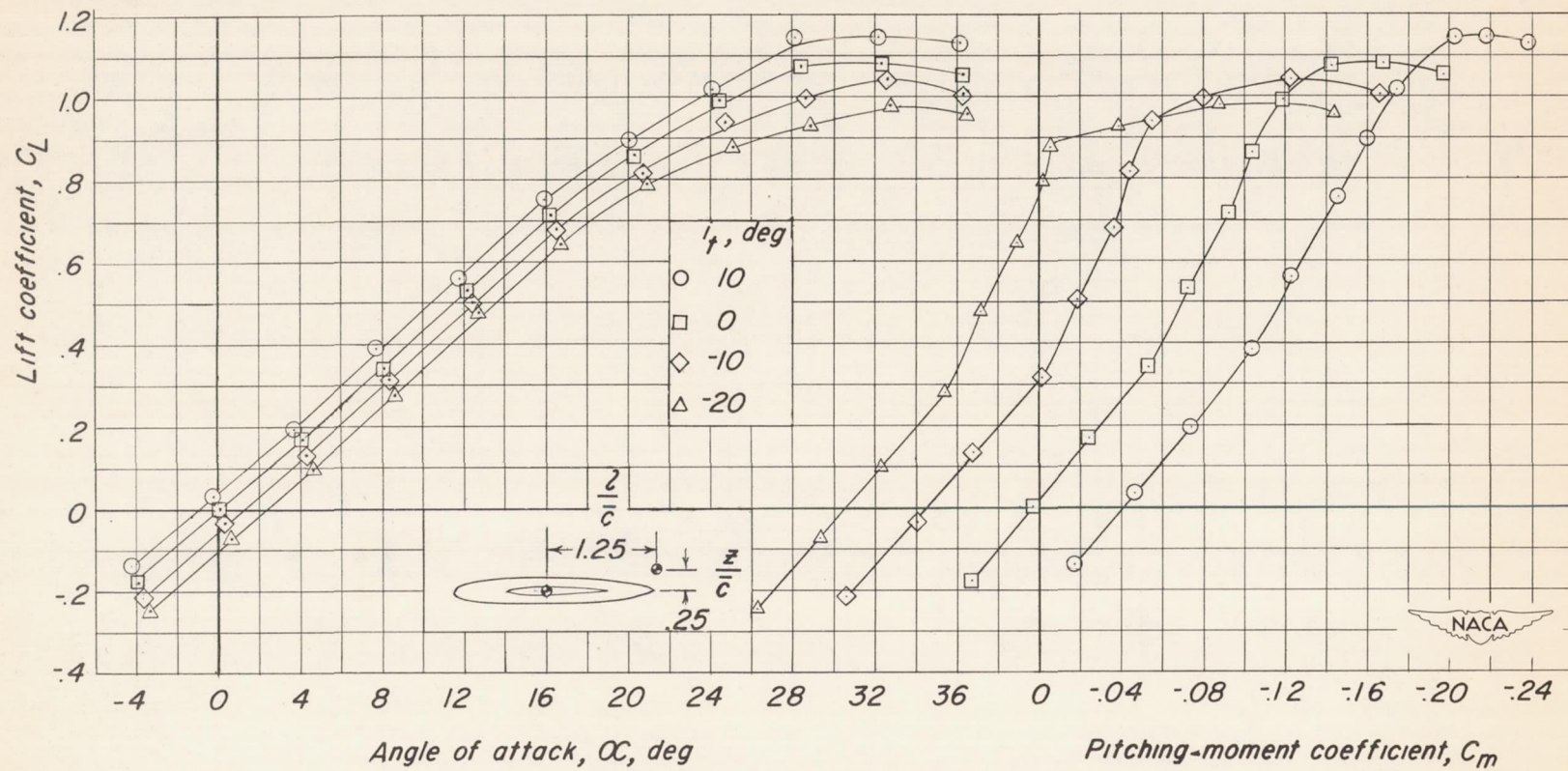
Figure 8.- Longitudinal stability and control characteristics of a 60° triangular-wing model having a triangular all-movable tail. H_2.
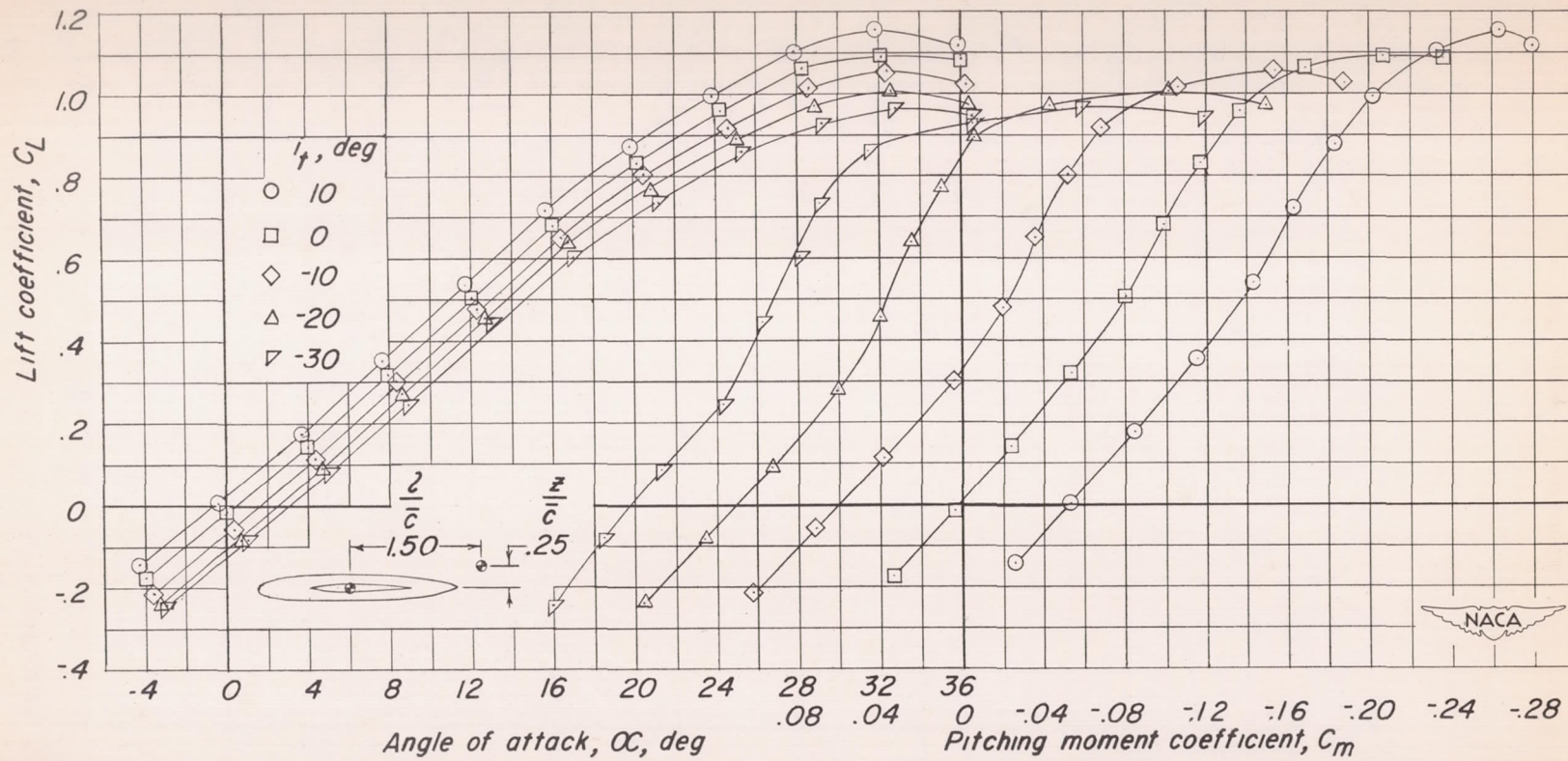
Figure 9.- Longitudinal stability and control characteristics of a
60° triangular-wing model having a triangular all-movable tail. H_2.
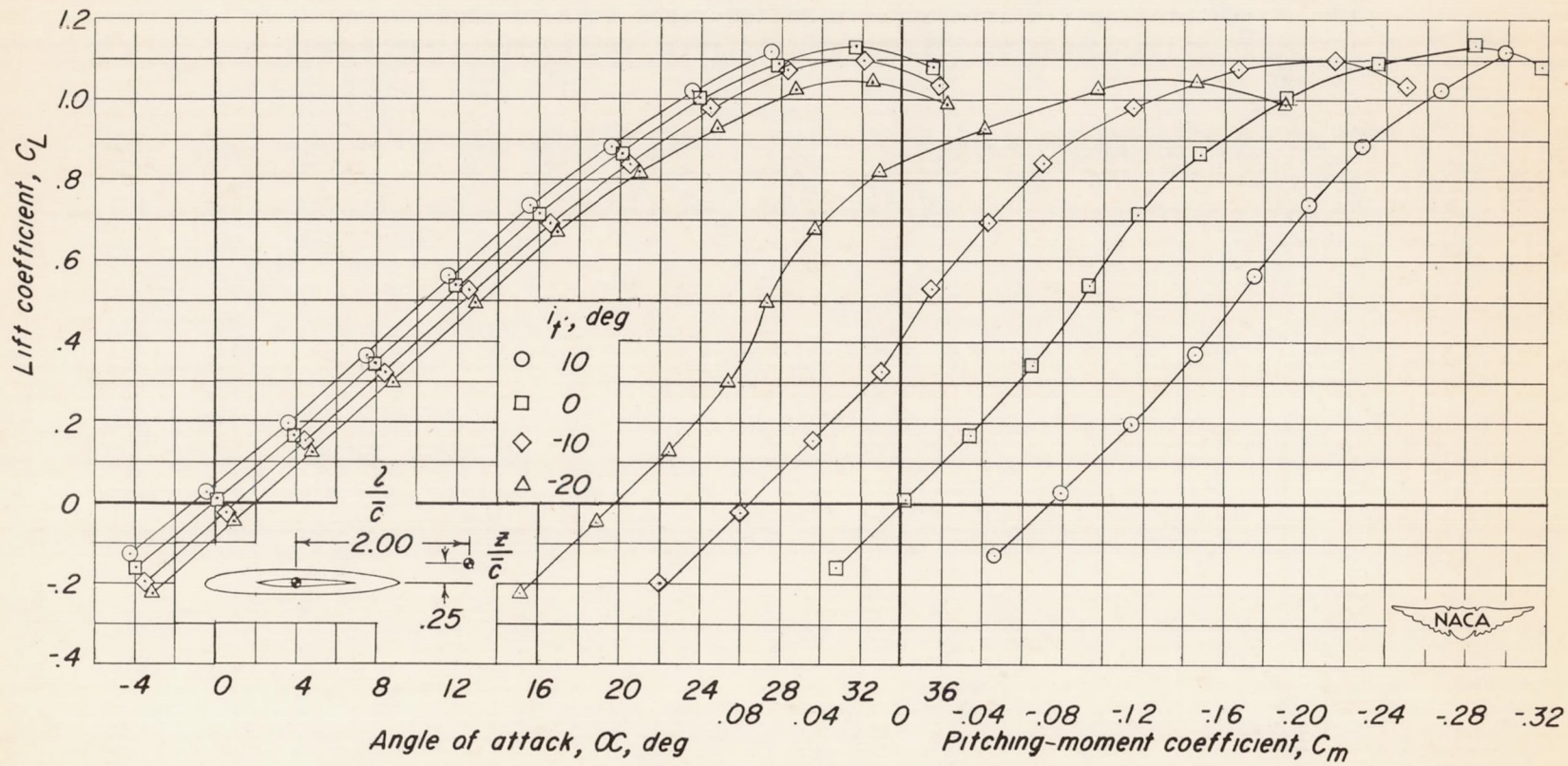
Figure 10.- Longitudinal stability and control characteristics of a 60° triangular-wing model having a triangular all-movable tail. H₂.
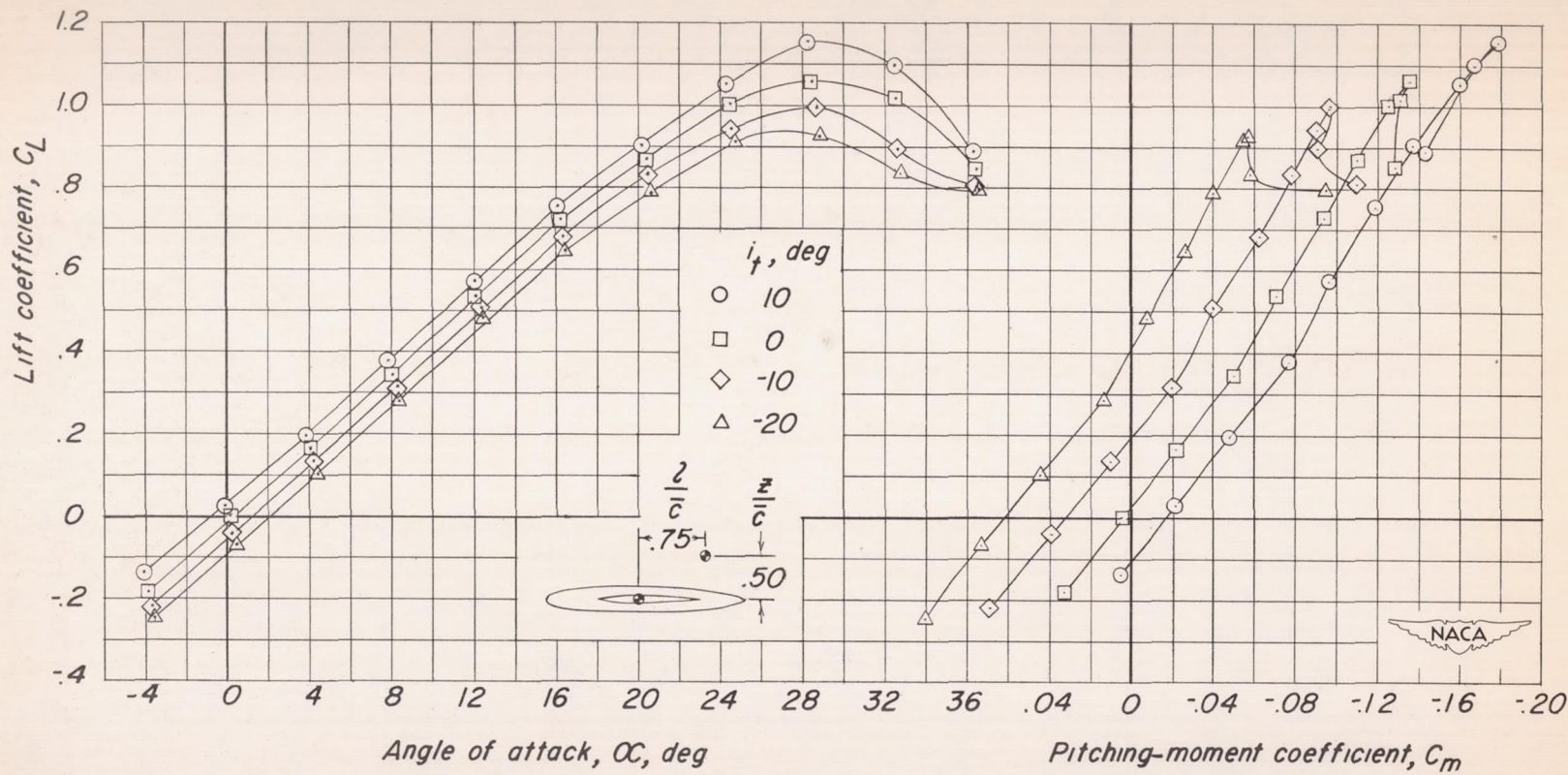
Figure 11.- Longitudinal stability and control characteristics of a 60° triangular-wing model having a triangular all-movable tail. H_2.
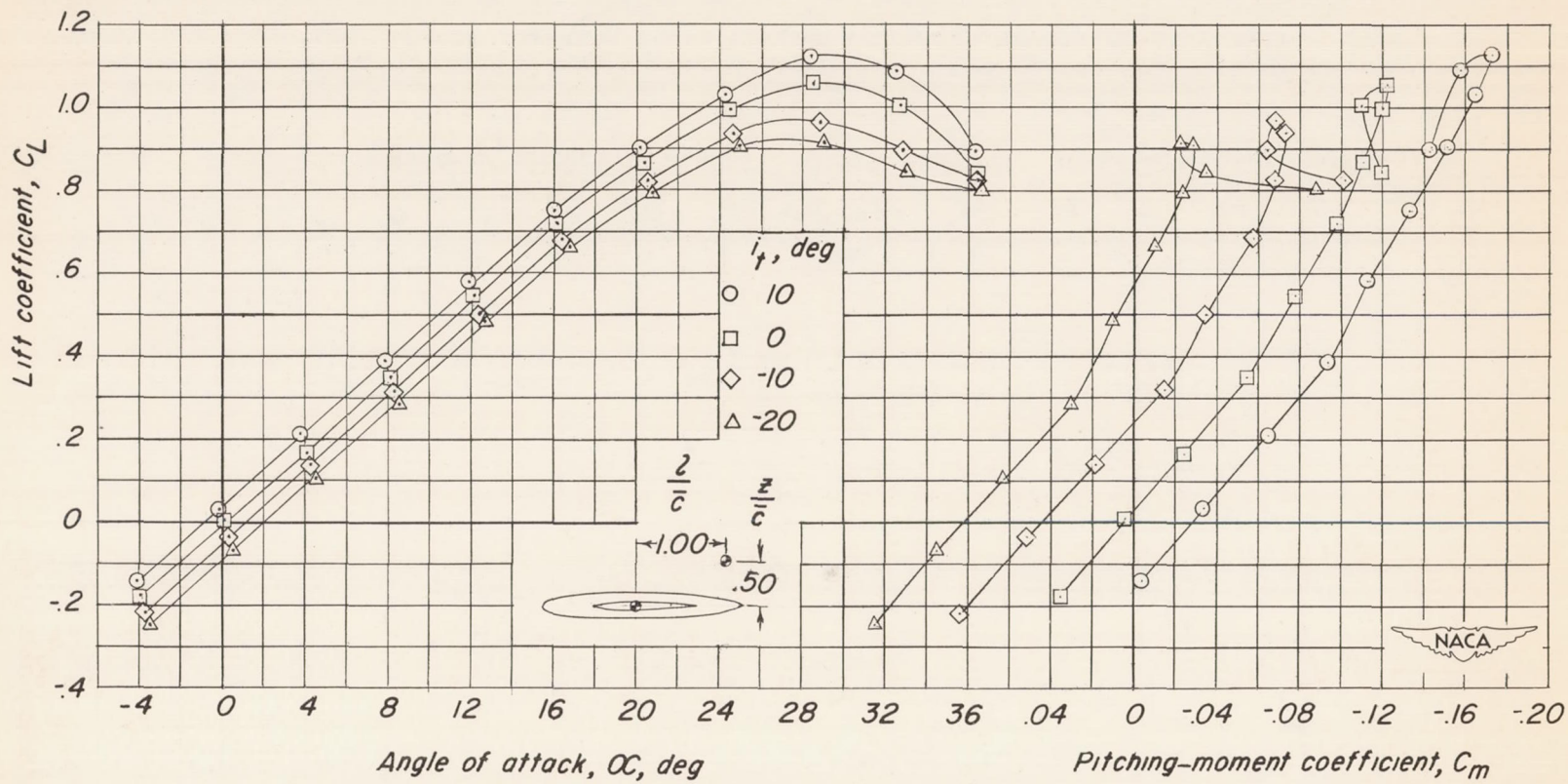
Figure 12.- Longitudinal stability and control characteristics of a 60° triangular-wing model having a triangular all-movable tail. H_2.
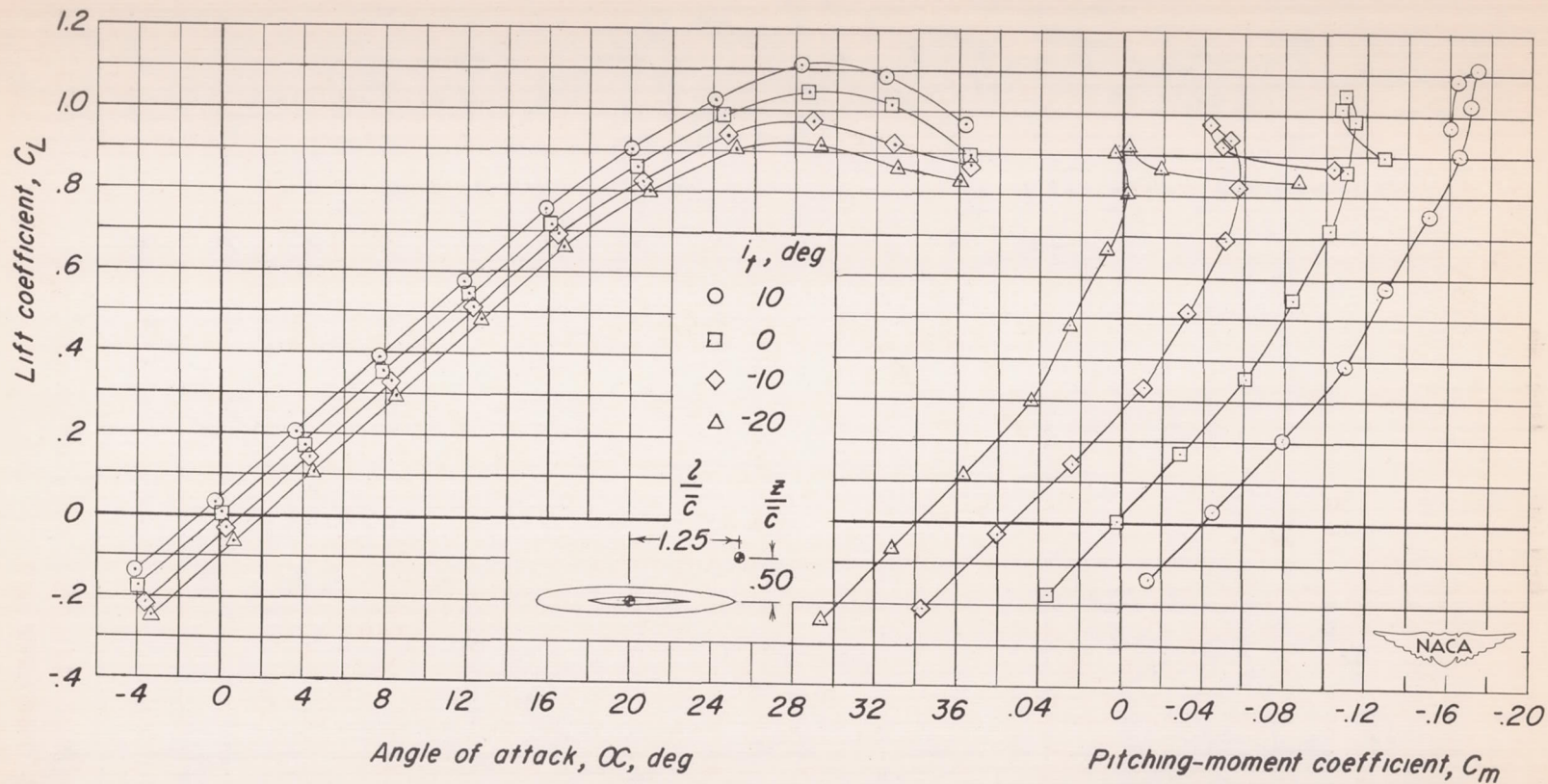
Figure 13.- Longitudinal stability and control characteristics of a
60°. triangular-wing model having a triangular all-movable tail. H_2.
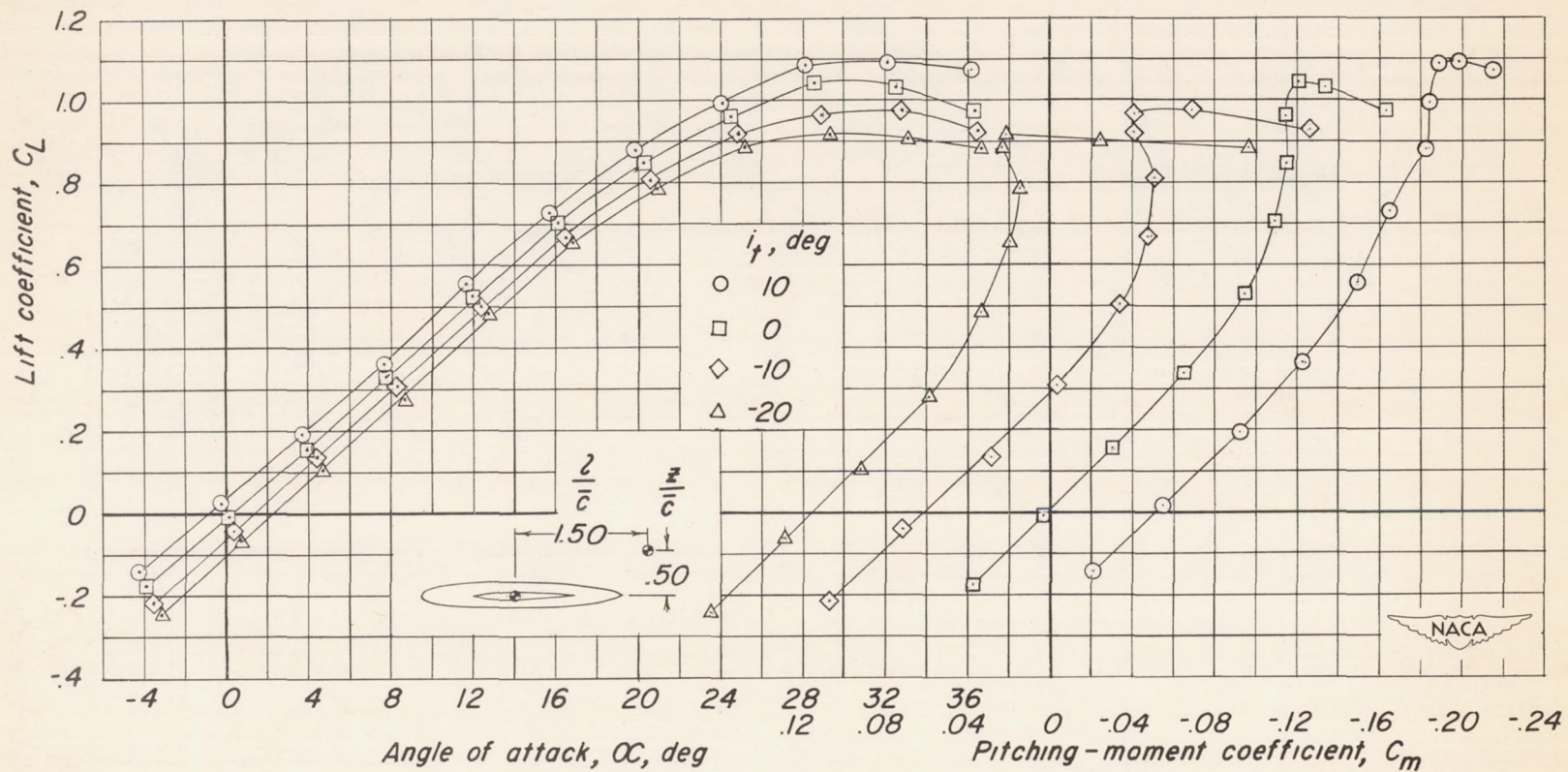
Figure 14.- Longitudinal stability and control characteristics of a
60° triangular-wing model having a triangular all-movable tail. H₂.
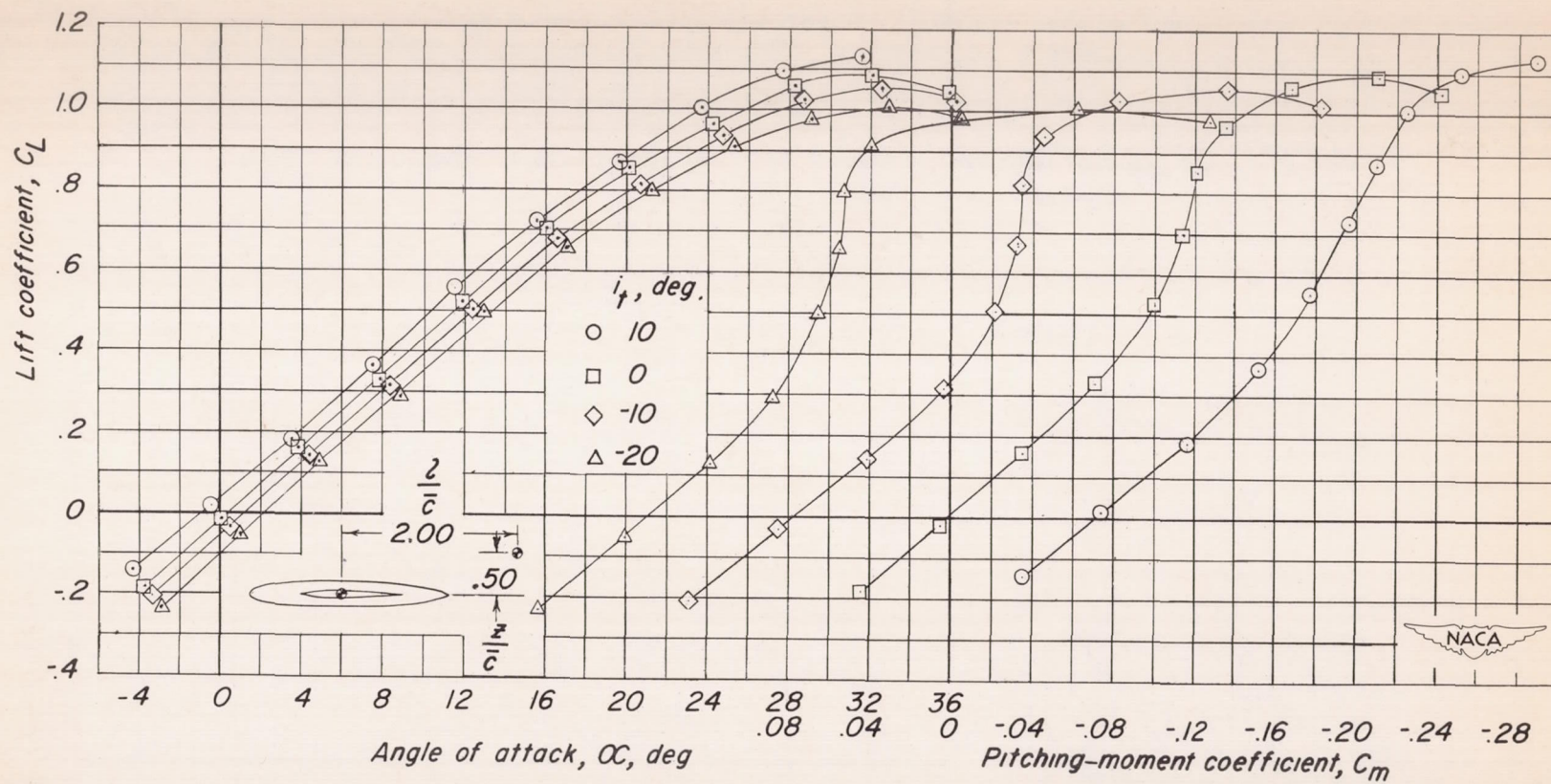
Figure 15.- Longitudinal stability and control characteristics of a
60° triangular-wing model having a triangular all-movable tail. H_2.
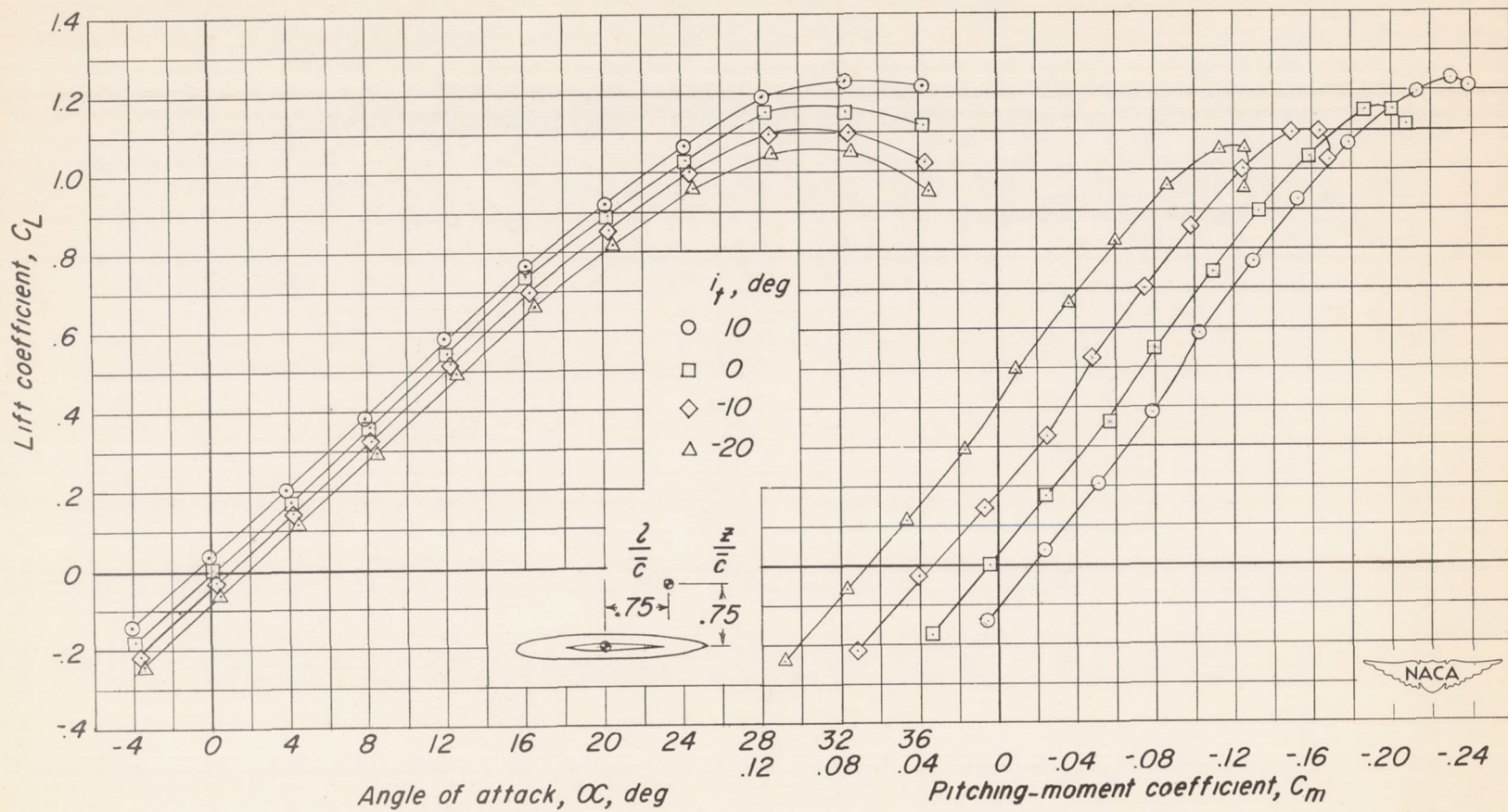
Figure 16.- Longitudinal stability and control characteristics of a
60° triangular-wing model having a triangular all-movable tail. H₂.
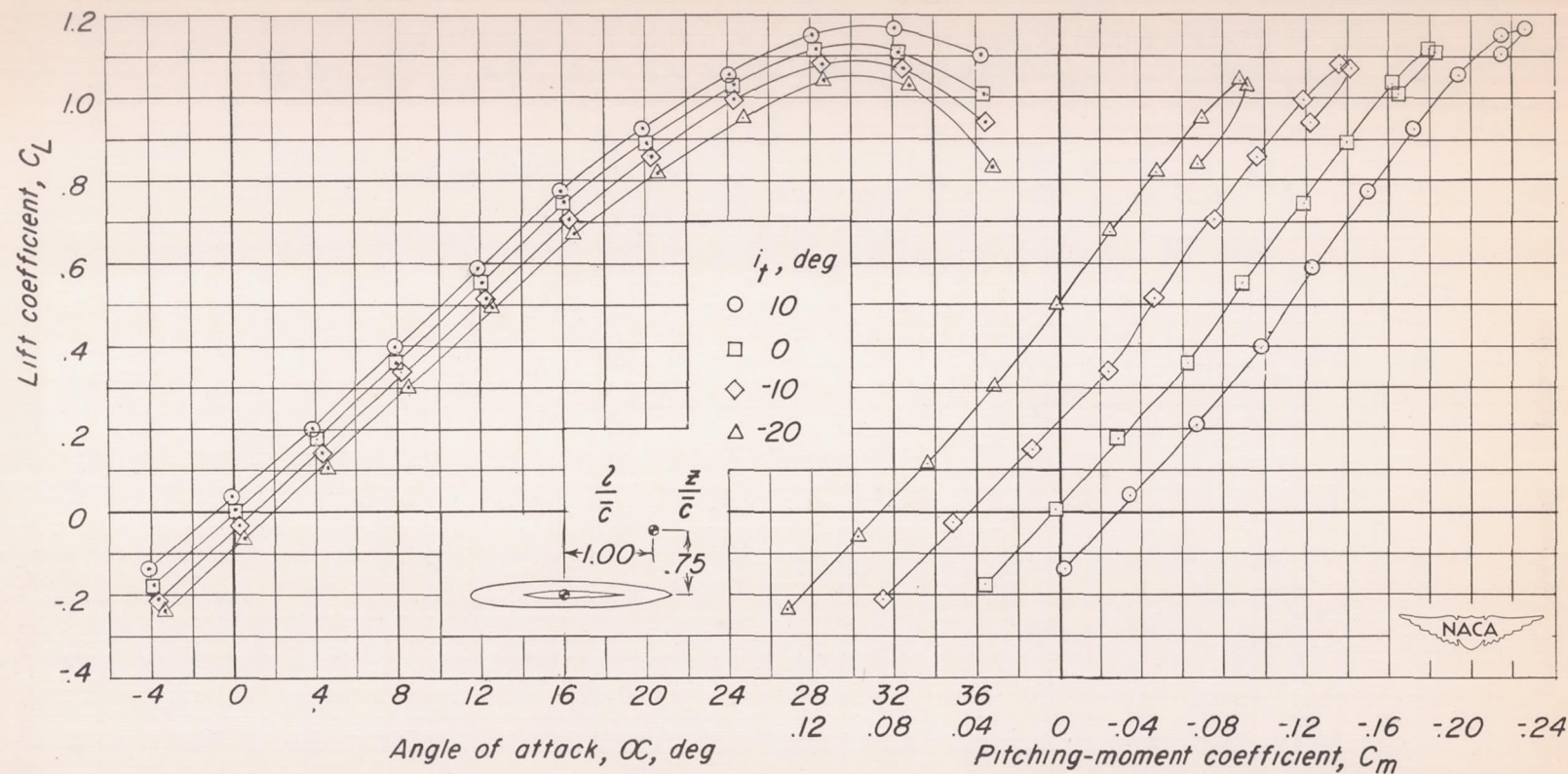
Figure 17.- Longitudinal stability and control characteristics of a
60° triangular-wing model having a triangular all-movable tail. H_2.
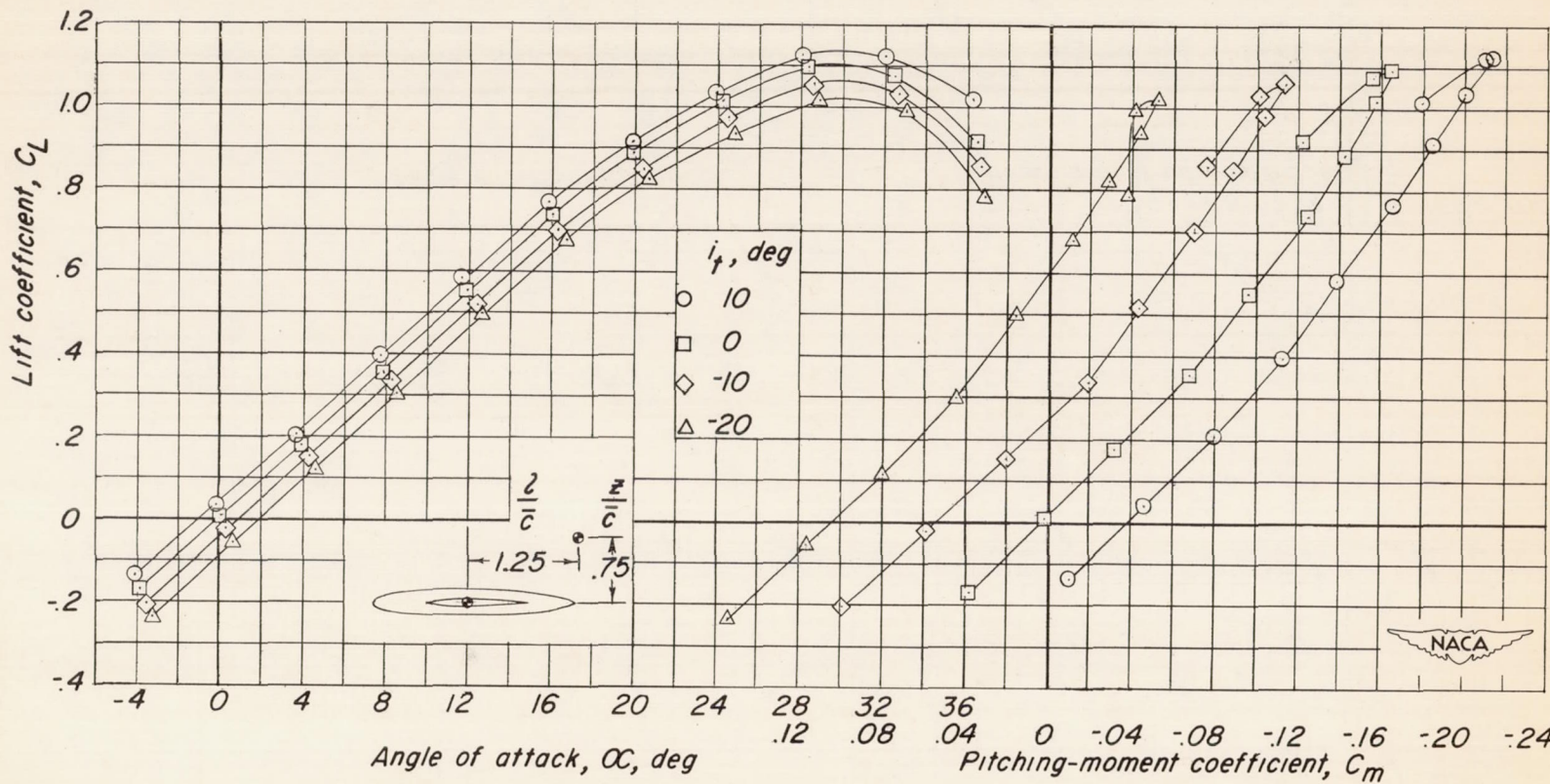
Figure 18.- Longitudinal stability and control characteristics of a
60° triangular-wing model having a triangular all-movable tail. H₂.
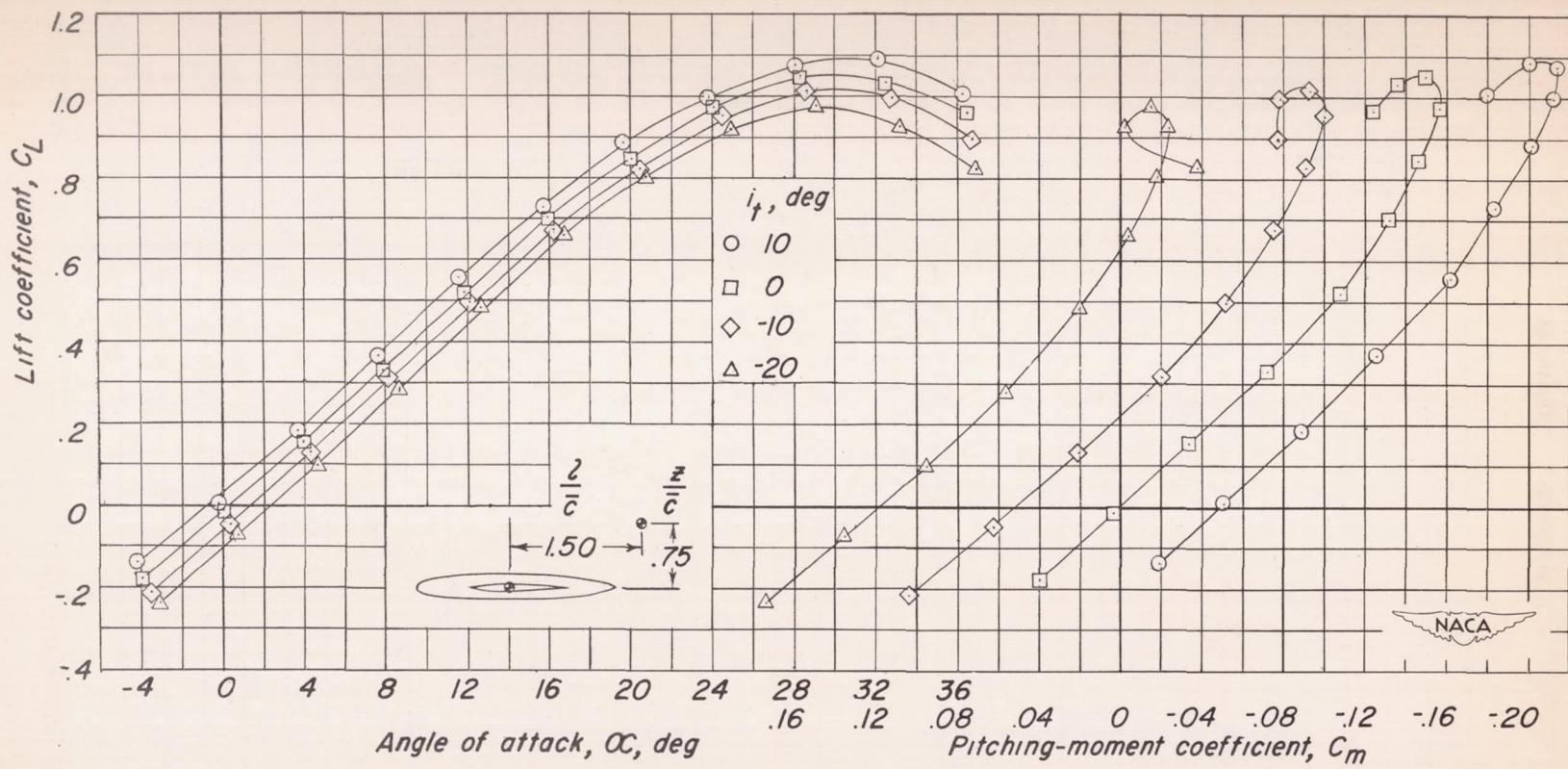
Figure 19.- Longitudinal stability and control characteristics of a
60° triangular-wing model having a triangular all-movable tail. H_2.
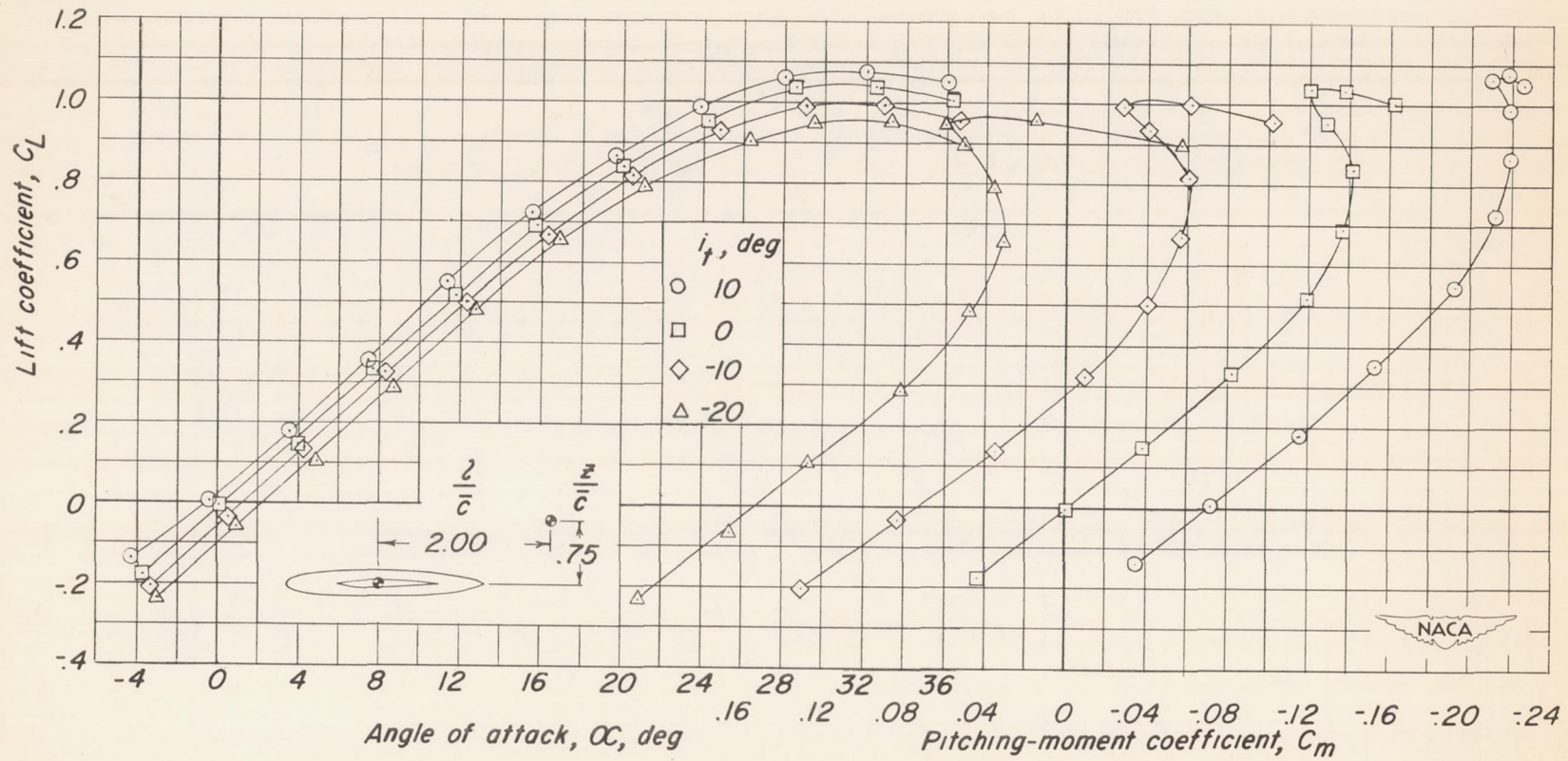
Figure 20.- Longitudinal stability and control characteristics of a 60° triangular-wing model having a triangular all-movable tail. H₂.
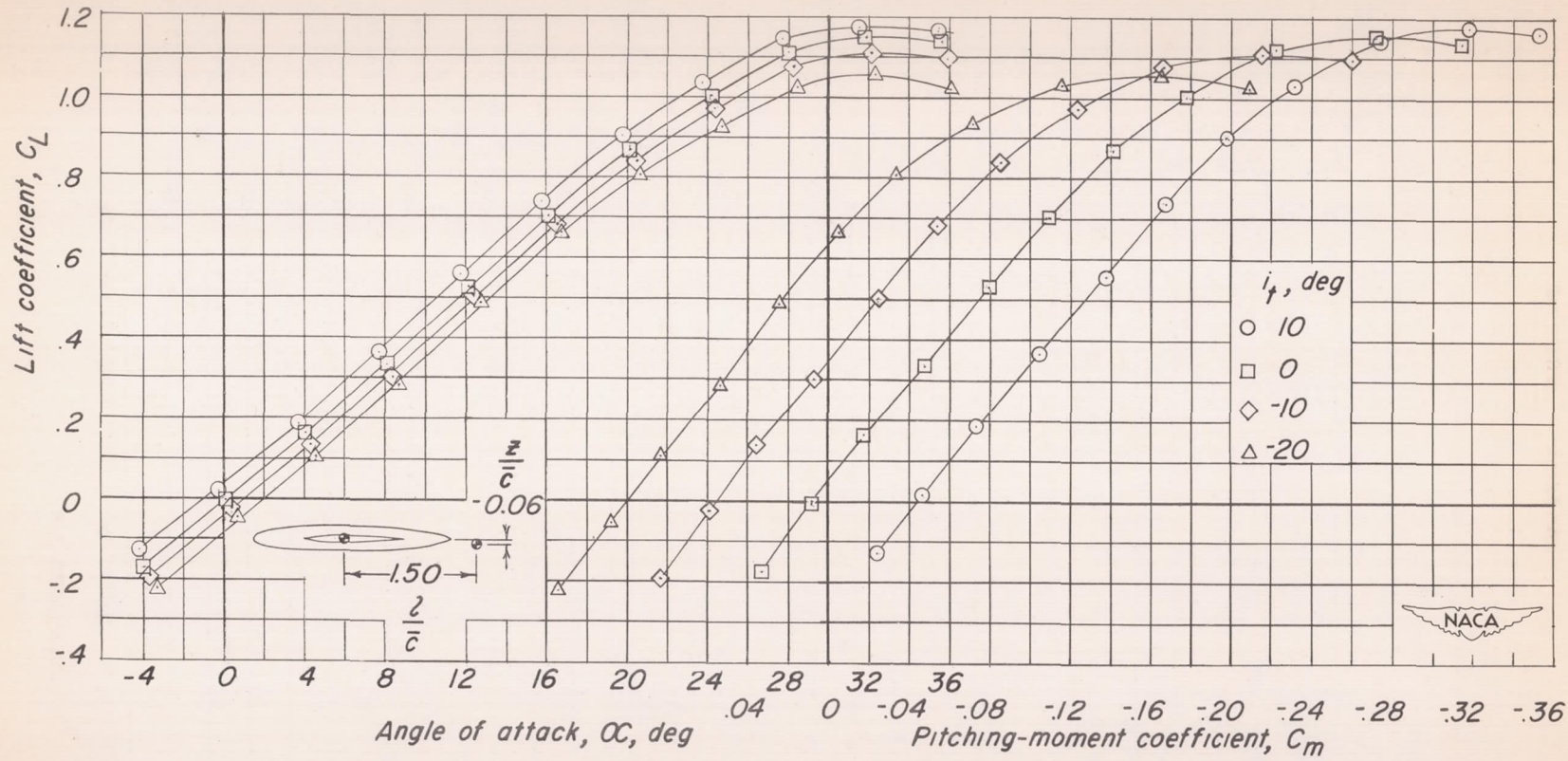
Figure 21.- Longitudinal stability and control characteristics of a
60° triangular-wing model having a triangular all-movable tail. H_2.
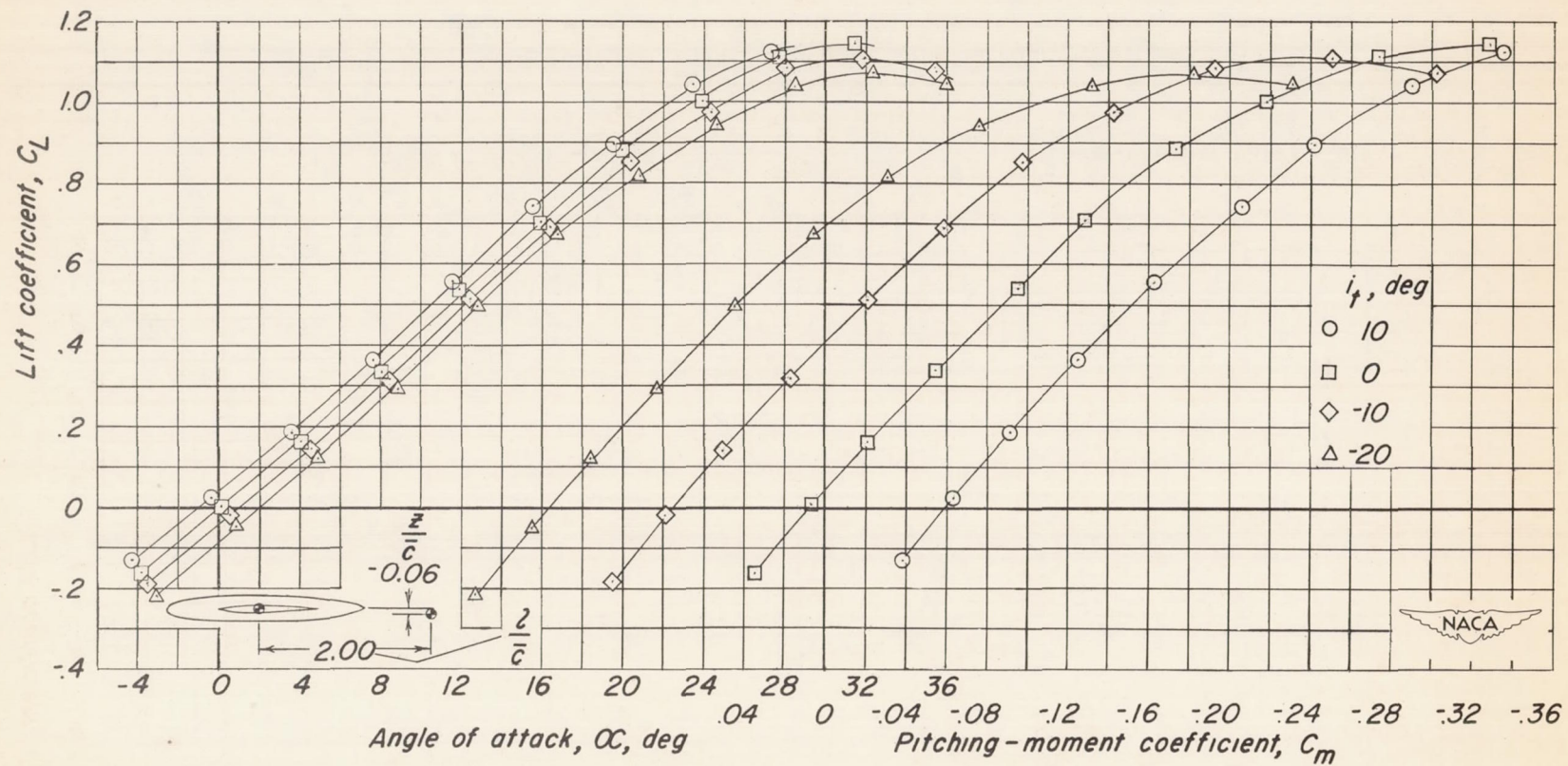
Figure 22.- Longitudinal stability and control characteristics of a
60° triangular-wing model having a triangular all-movable tail. H_2.
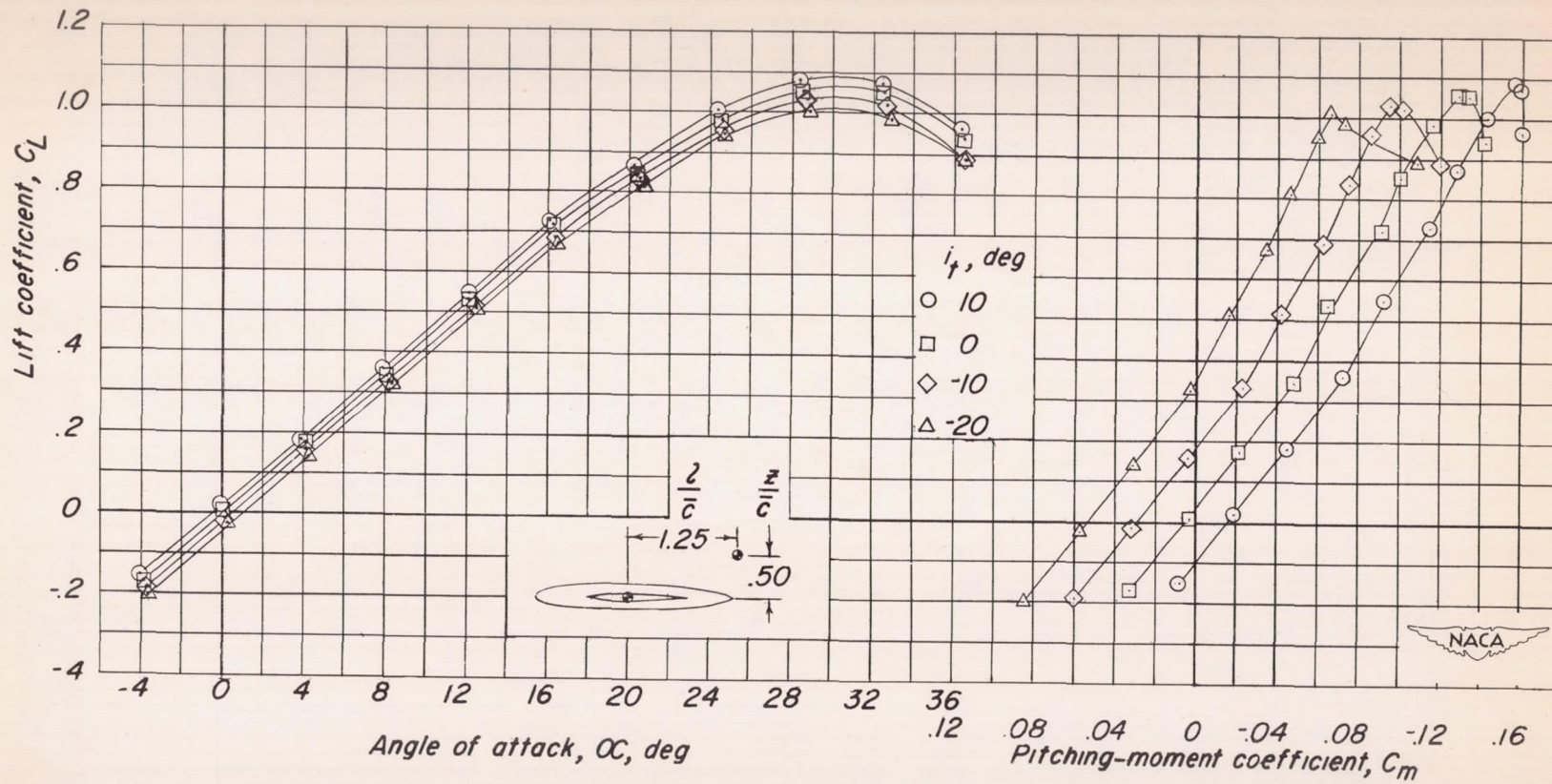
Figure 23.- Longitudinal stability and control characteristics of a
60° triangular-wing model having a triangular all-movable tail. H₁.
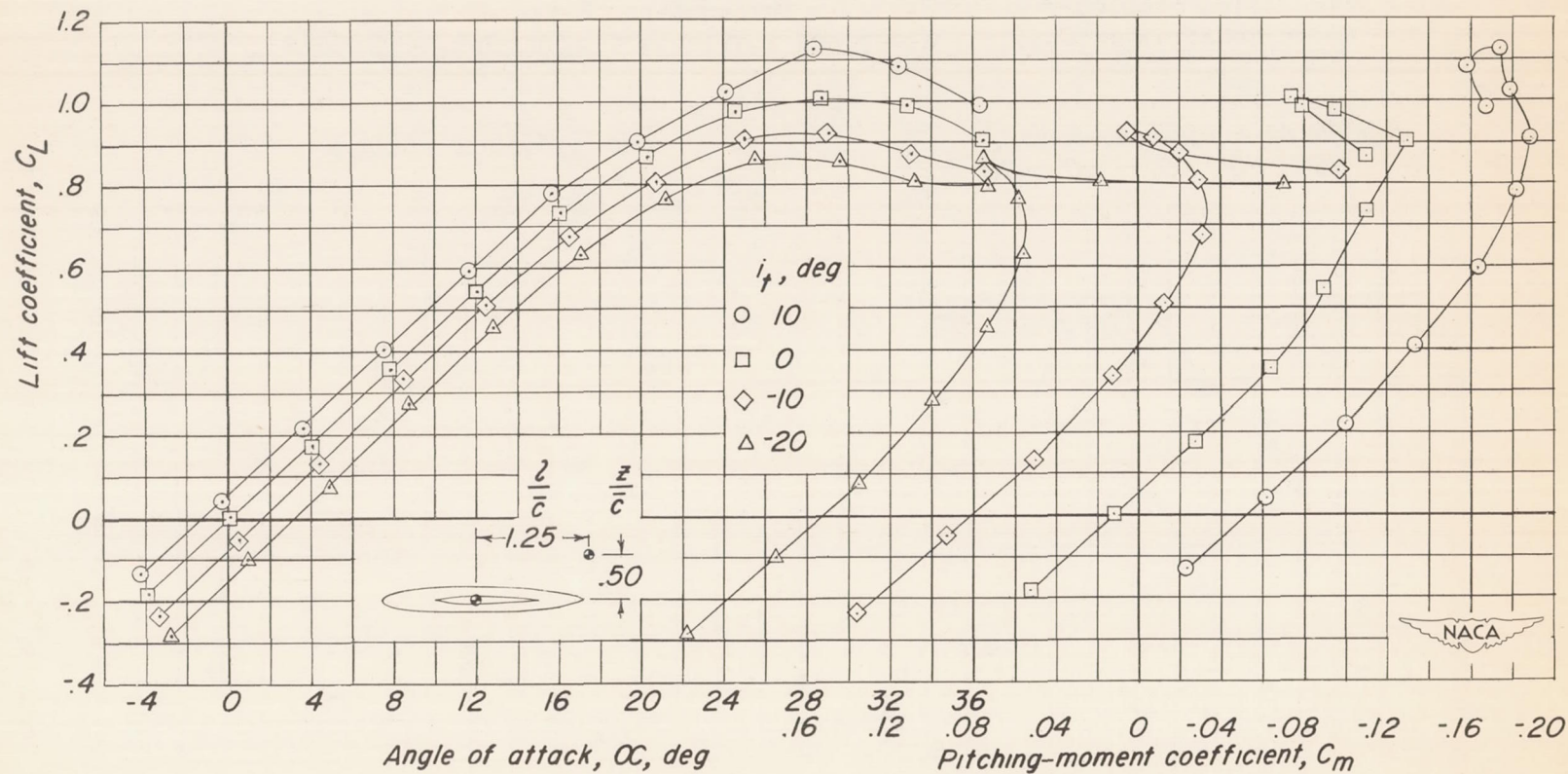
Figure 24.- Longitudinal stability and control characteristics of a 60° triangular-wing model having a triangular all-movable tail. H_3.
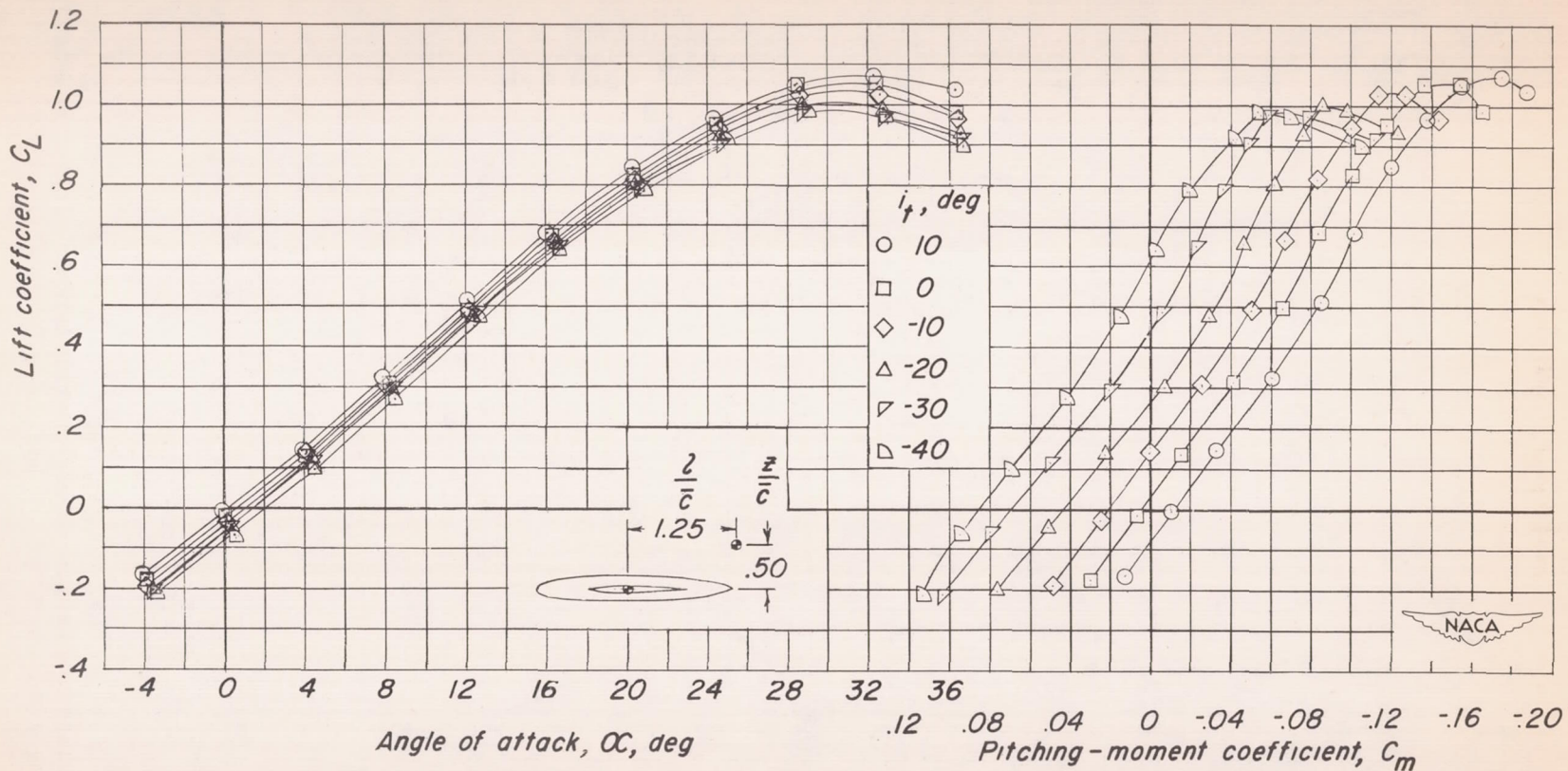
Figure 25.- Longitudinal stability and control characteristics of a
60° triangular-wing model having a triangular all-movable tail. H₄.
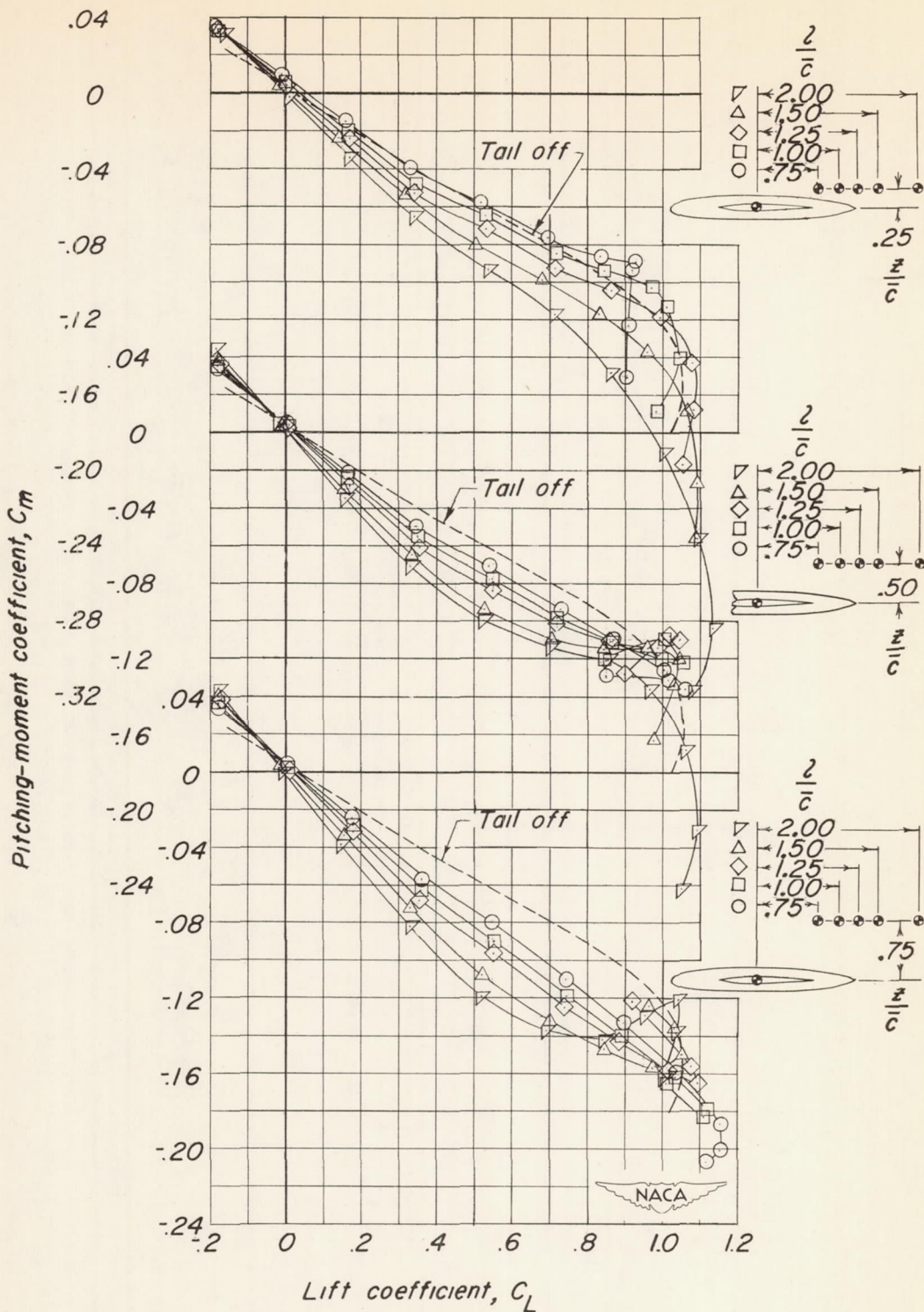
Figure 26.- Effect of tail length and tail height on static longitudinal stability characteristics of a 60° triangular-wing model having a triangular all-movable tail. H_2; $i_t = 0°$.
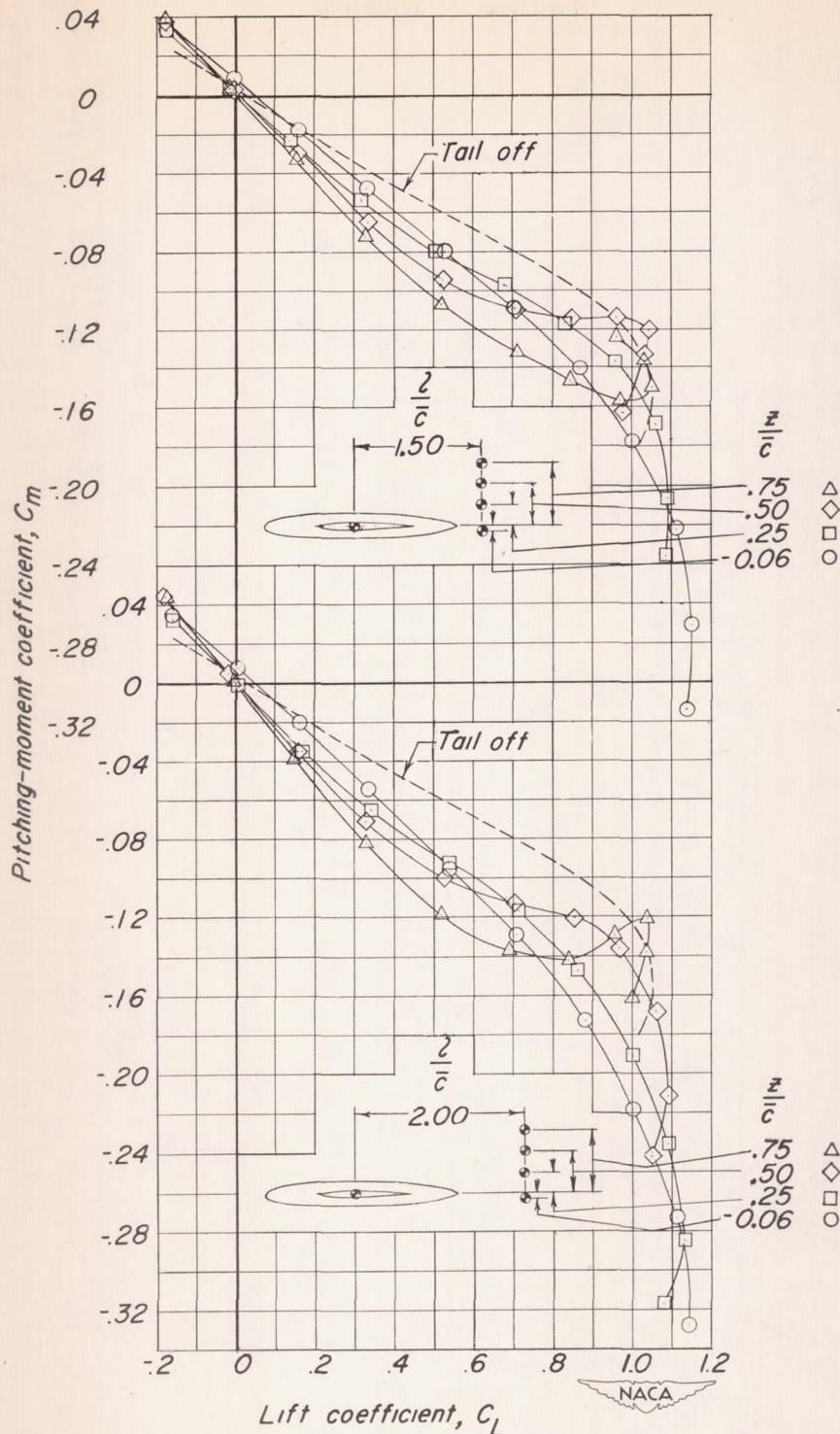
Figure 27.- Effect of tail height on static longitudinal stability characteristics of a 60° triangular-wing model having a triangular all-movable tail. H_2; $i_t = 0^\circ$.
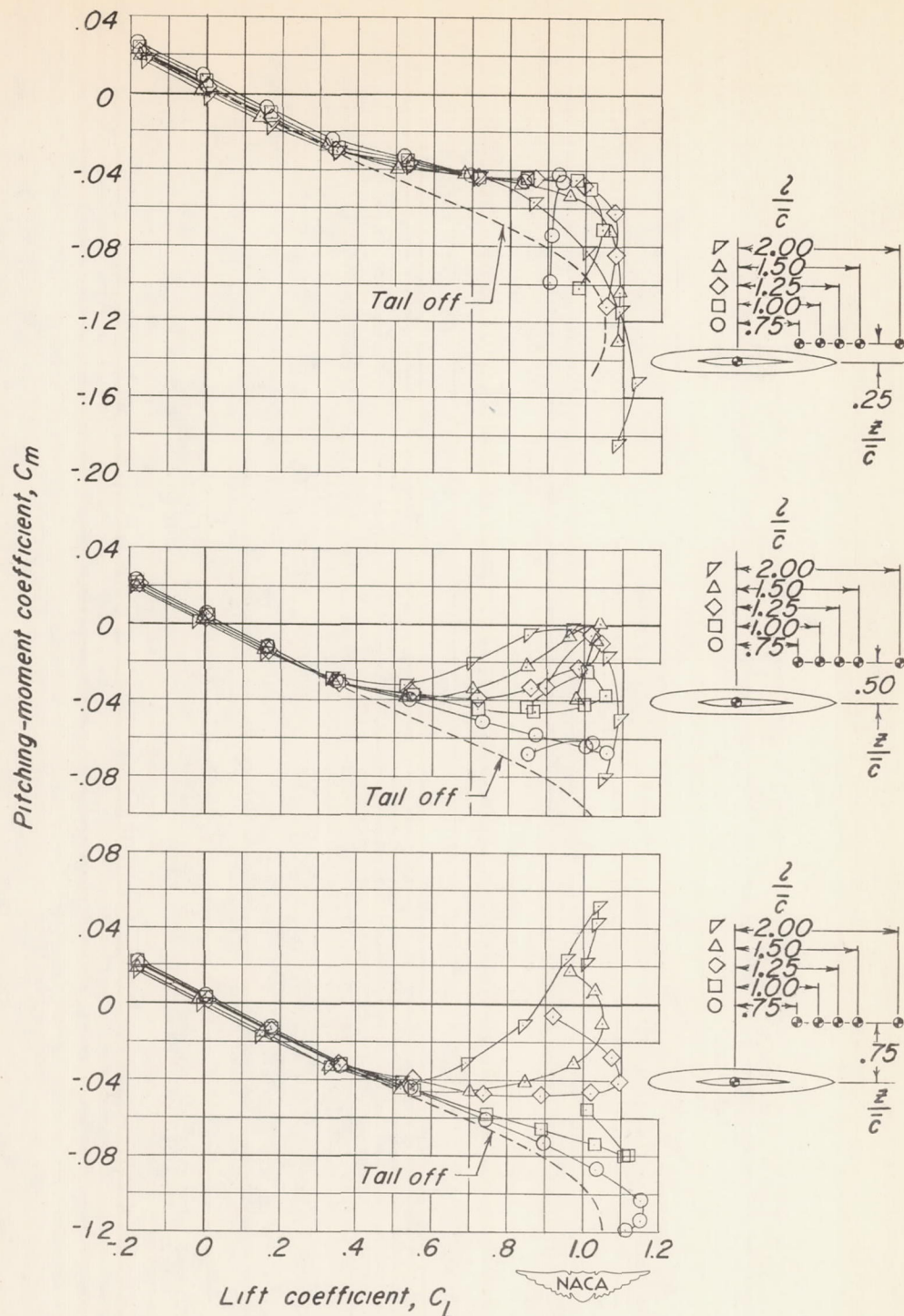
Figure 28.- Effect of tail length and tail height on static longitudinal stability characteristics of a 60° triangular-wing model having a triangular all-movable tail. H_2; $C_{m_{C_L}} = -0.10$; $i_t = 0°$. (See text for centers of gravity.)
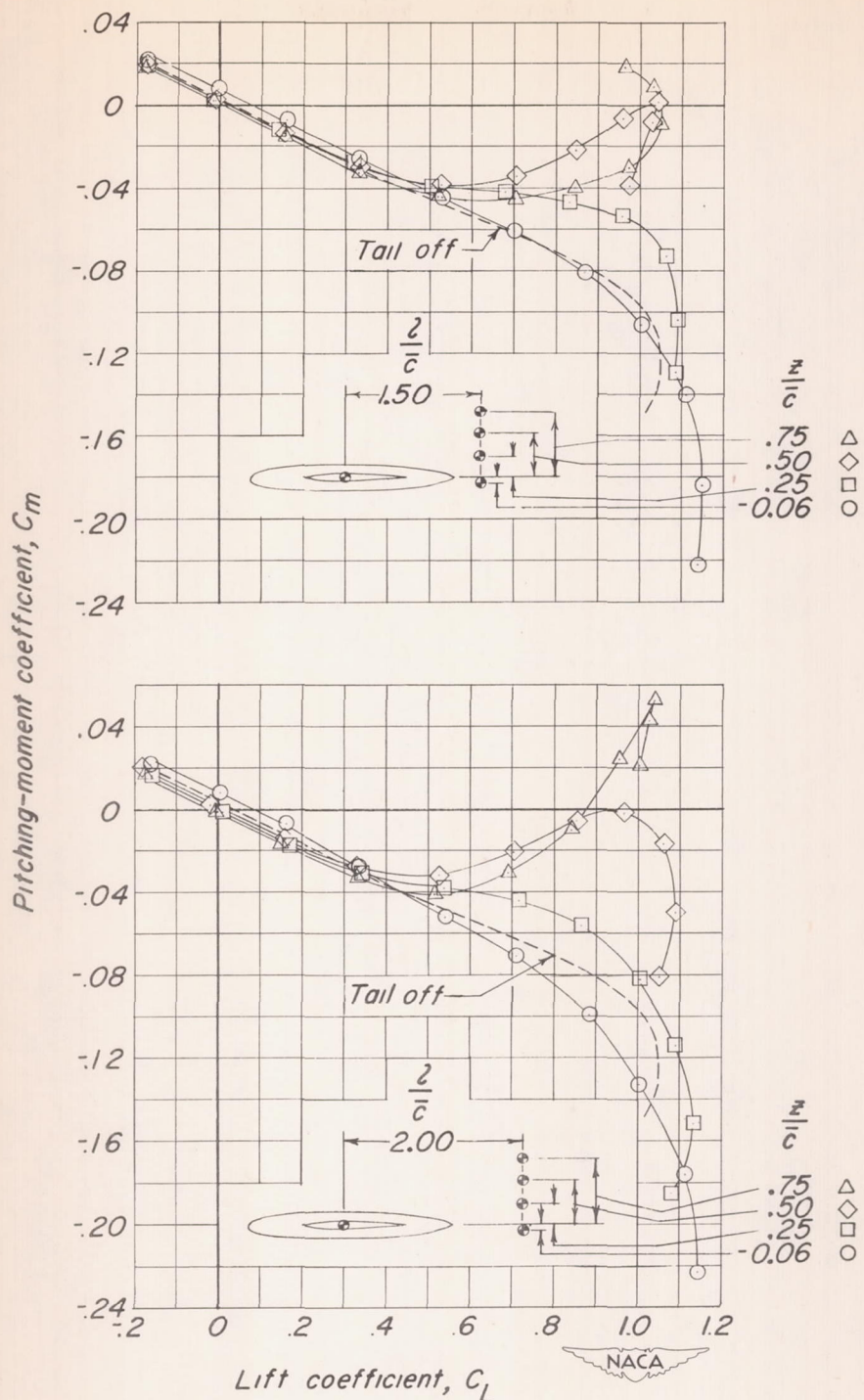
Figure 29.- Effect of tail height on static longitudinal stability characteristics of a 60° triangular-wing model having a triangular all-movable tail. H_2; $C_{m_{C_L}} = -0.10$; $i_t = 0°$. (See text for centers of gravity.)

Maximum change in $\partial C_m / \partial C_L$ between $C_L = 0$ and $C_L = 0.8$

Less than $0.05\,\bar{c}$

Between $0.05\,\bar{c}$ and $0.10\,\bar{c}$

Between $0.10\,\bar{c}$ and $0.15\,\bar{c}$

More than $0.15\,\bar{c}$

$z/\bar{c}$

.8

.6

.4

.2

0

-.2

NACA

$l/\bar{c}$

0   .2   .4   .6   .8   1.0   1.2   1.4   1.6   1.8   2.0
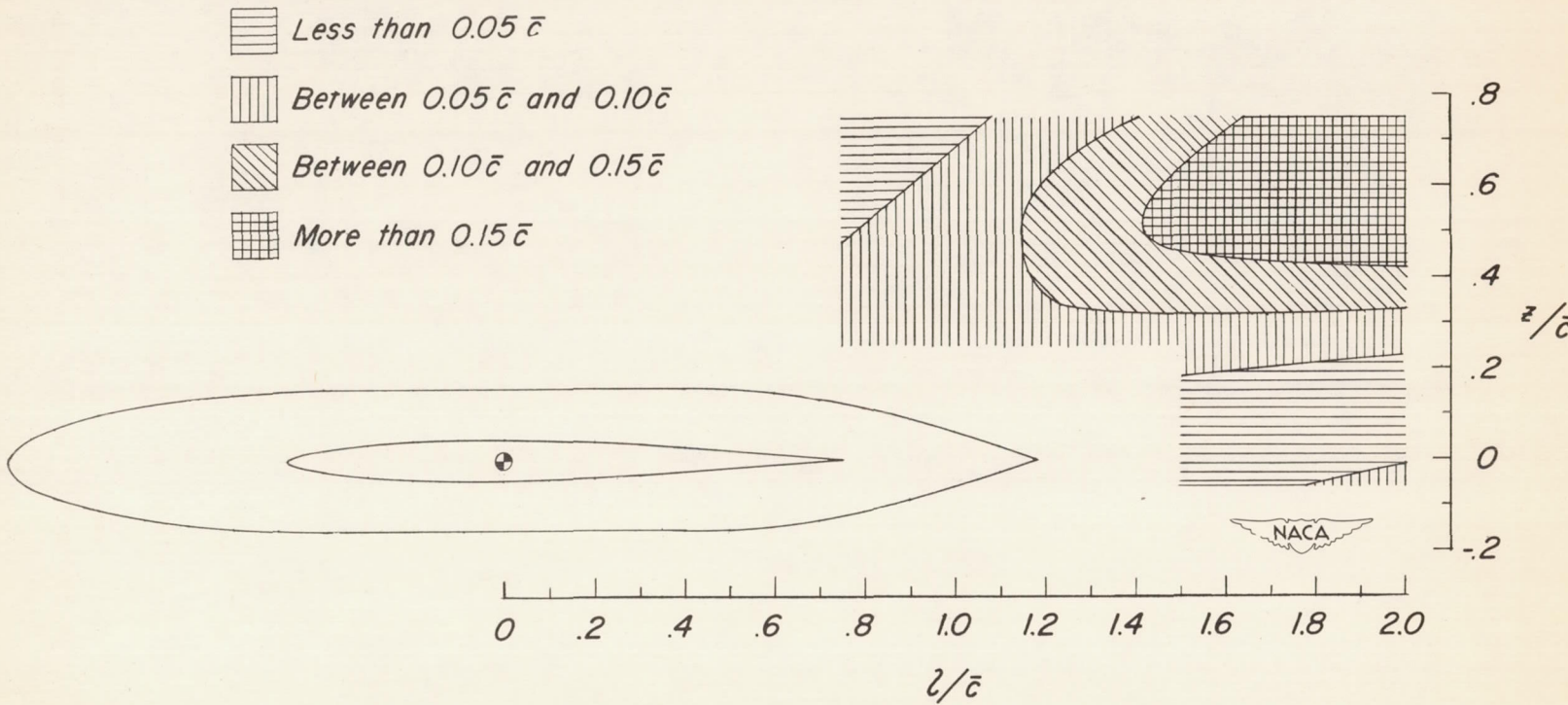
Figure 30.- Summary of effect of horizontal-tail location on longitudinal stability. H_2; $i_t = 0^o$.
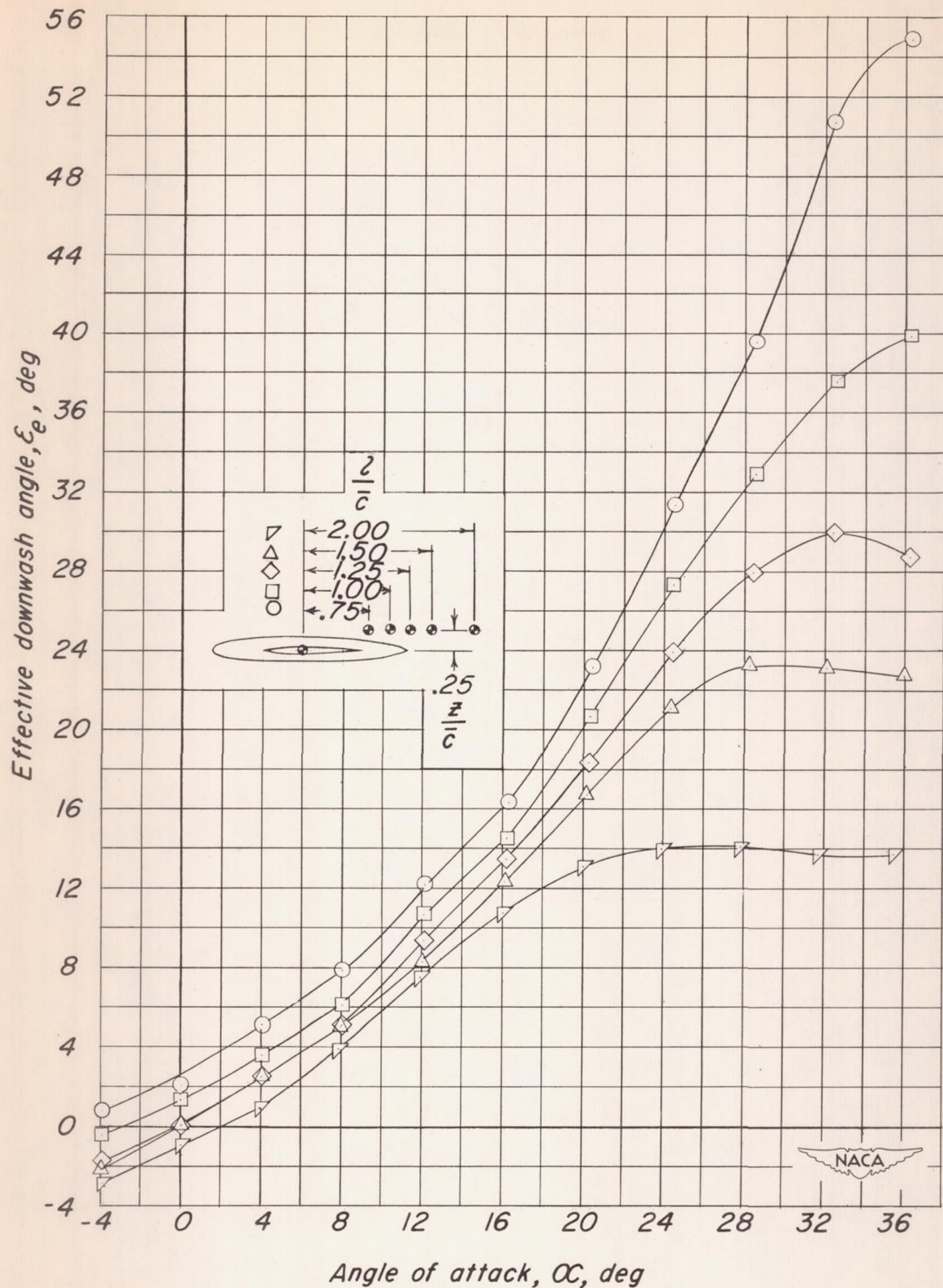
Figure 31.- Effect of tail length on variation of effective downwash angle with angle of attack for a 60° triangular-wing model having a triangular all-movable tail. H_2; $i_t = 0^\circ$.
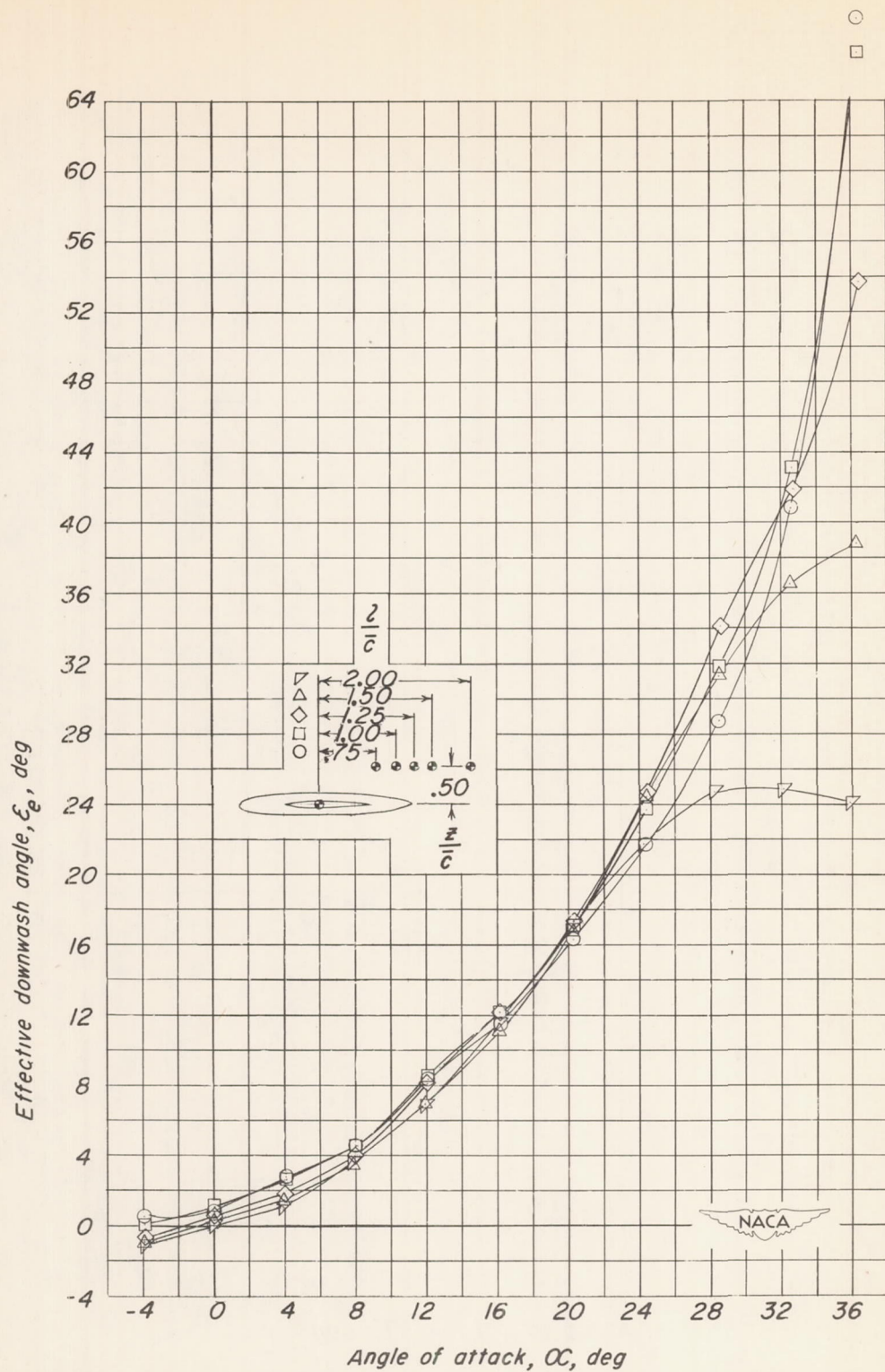
Figure 32.- Effect of tail length on variation of effective downwash angle with angle of attack for a 60° triangular-wing model having a triangular all-movable tail. H_2; $i_t = 0^{\circ}$.
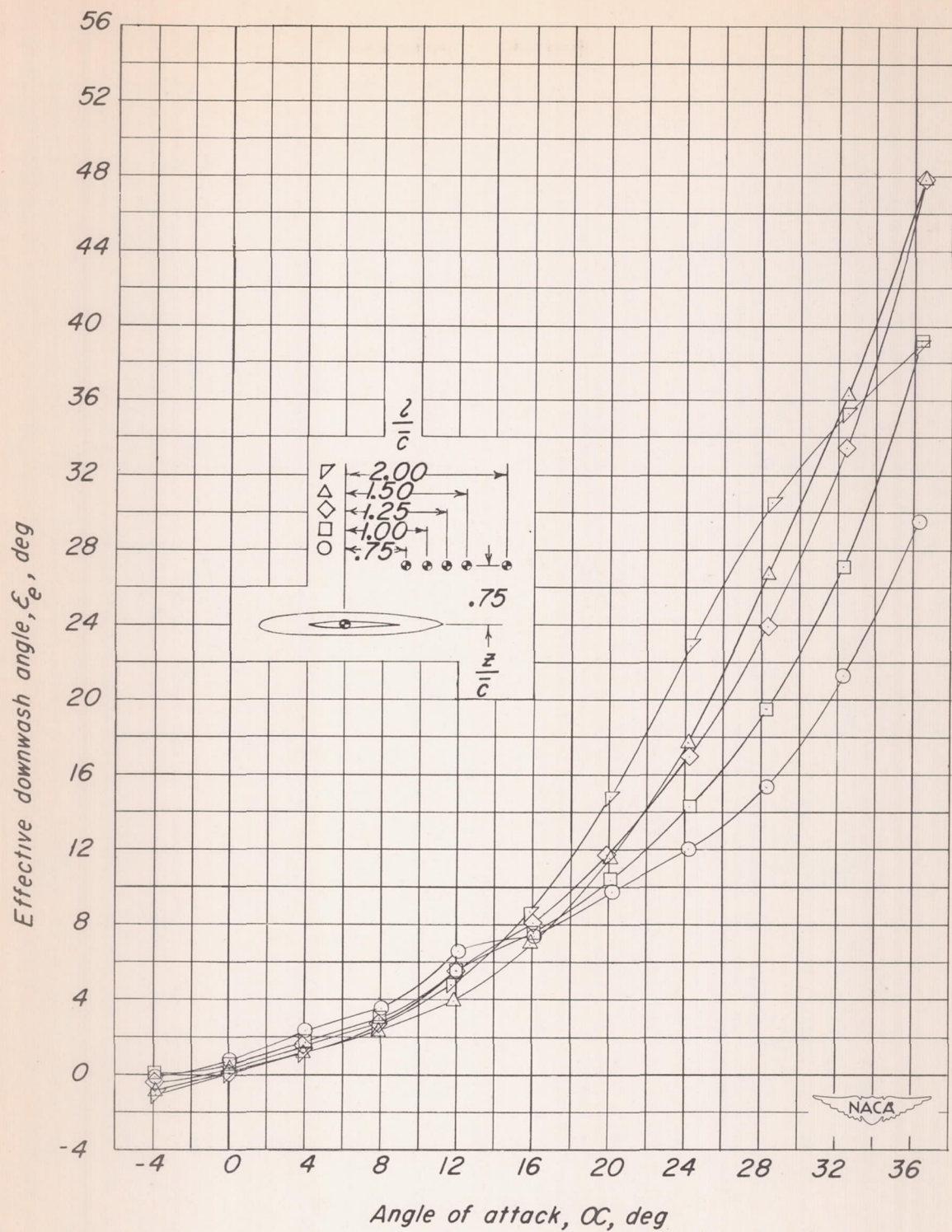
Figure 33.- Effect of tail length on variation of effective downwash angle with angle of attack for a 60° triangular-wing model having a triangular all-movable tail. H_2; $i_t = 0^\circ$.
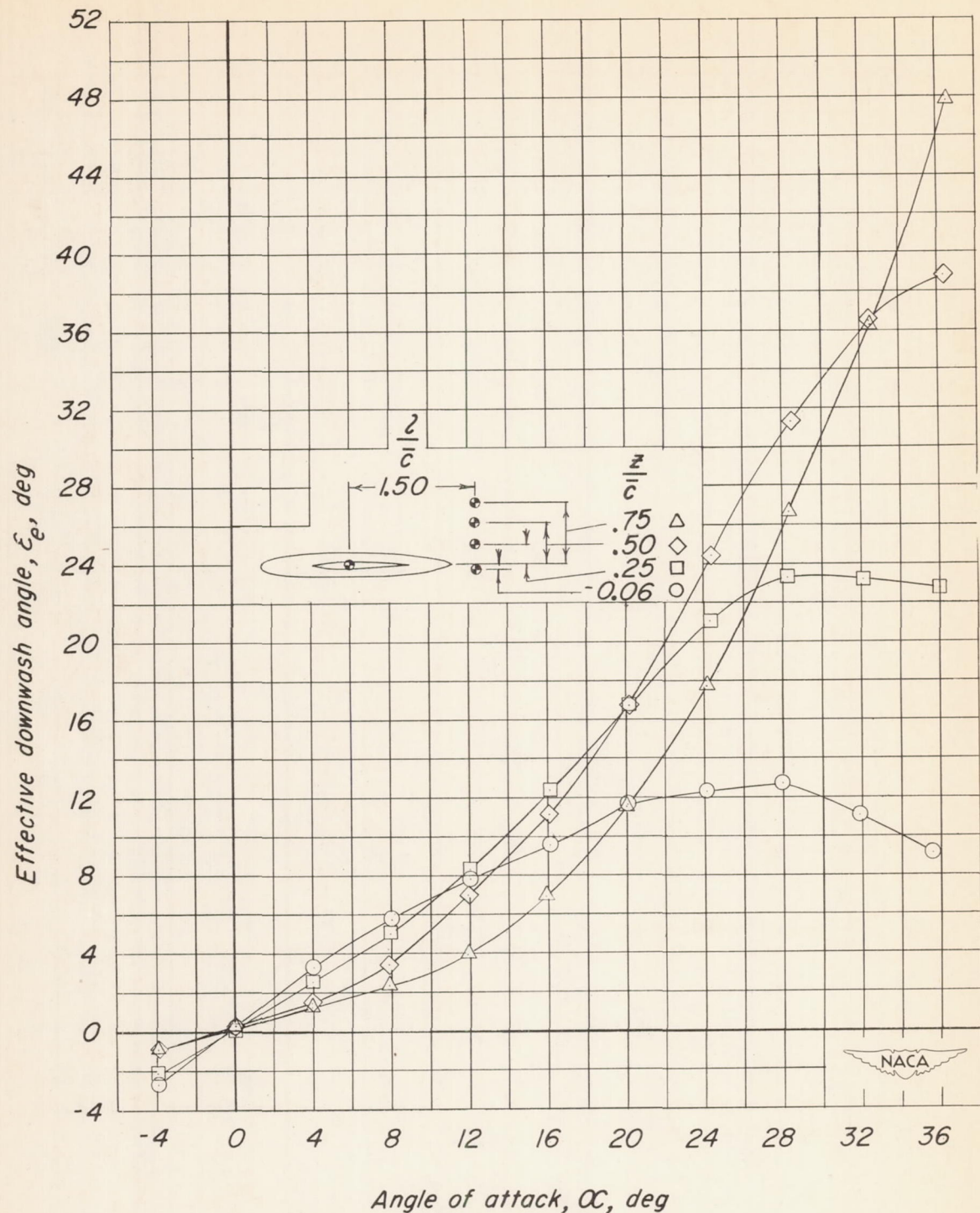
Figure 34.- Effect of tail height on variation of effective downwash angle with angle of attack for a 60° triangular-wing model having a triangular all-movable tail. H₂; $i_t = 0°$.
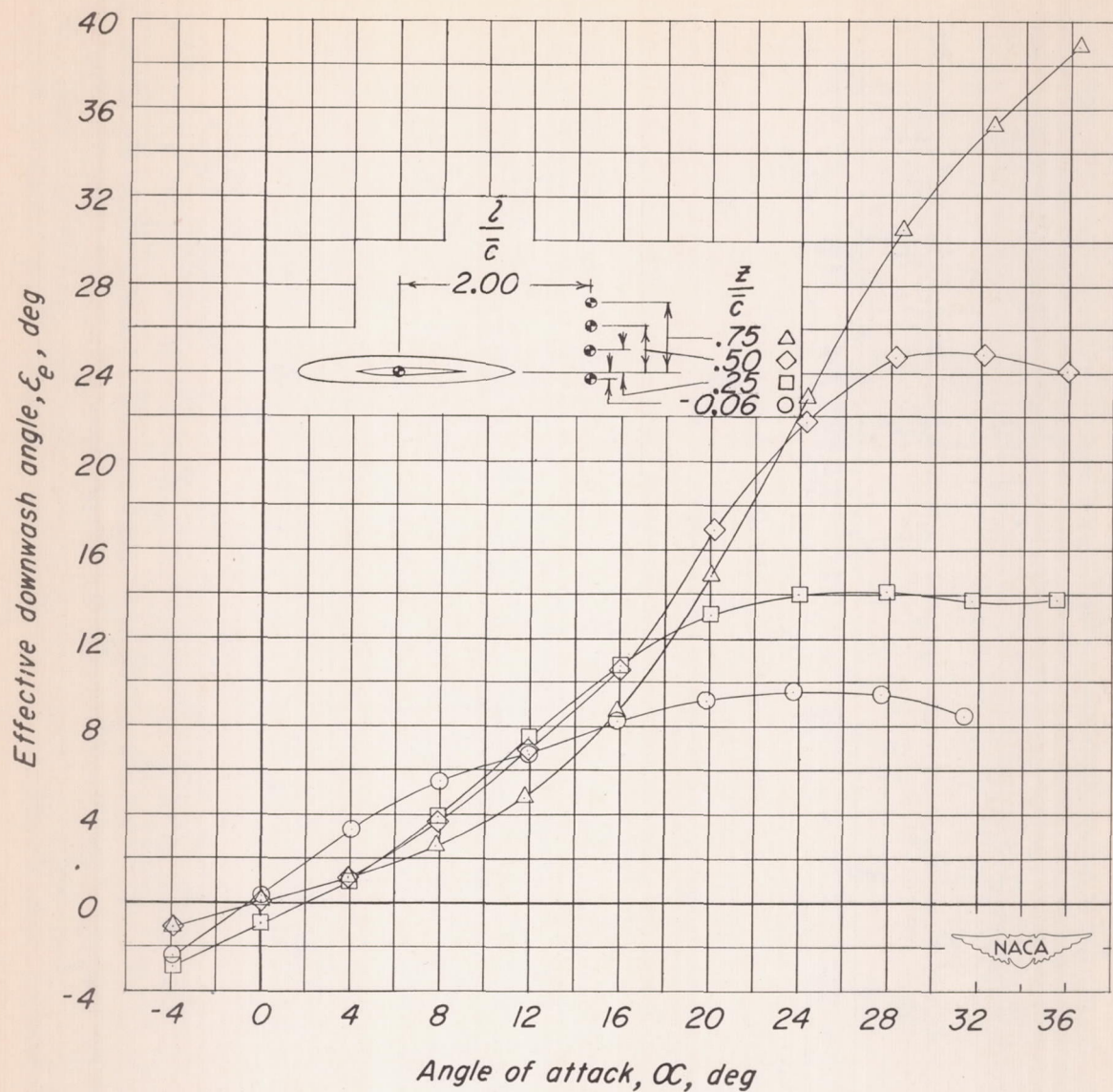
Figure 35.- Effect of tail height on variation of effective downwash
angle with angle of attack for a $60°$ triangular-wing model having
a triangular all-movable tail. H_2; $i_t = 0°$.
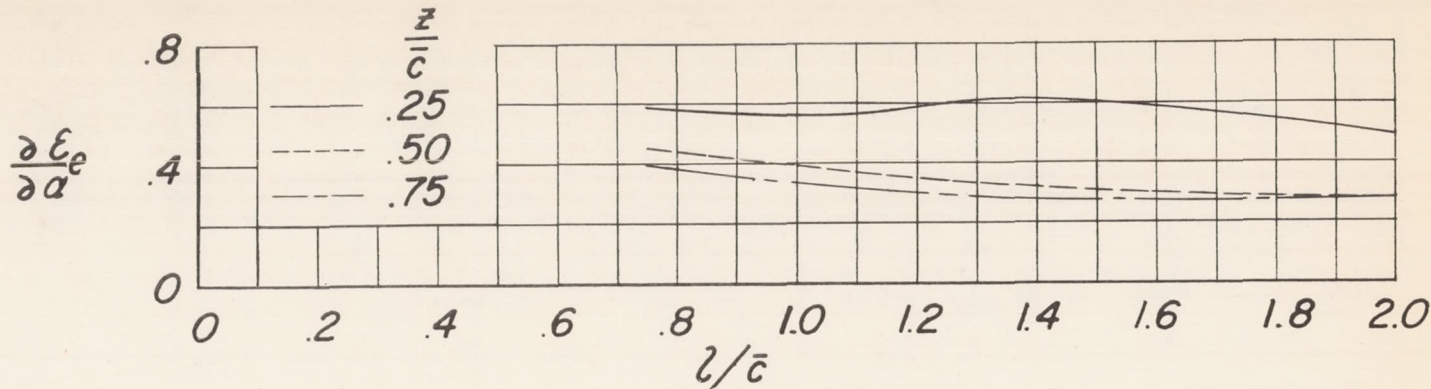
(a) $\partial\epsilon_e/\partial\alpha$ against $l/\bar{c}$.
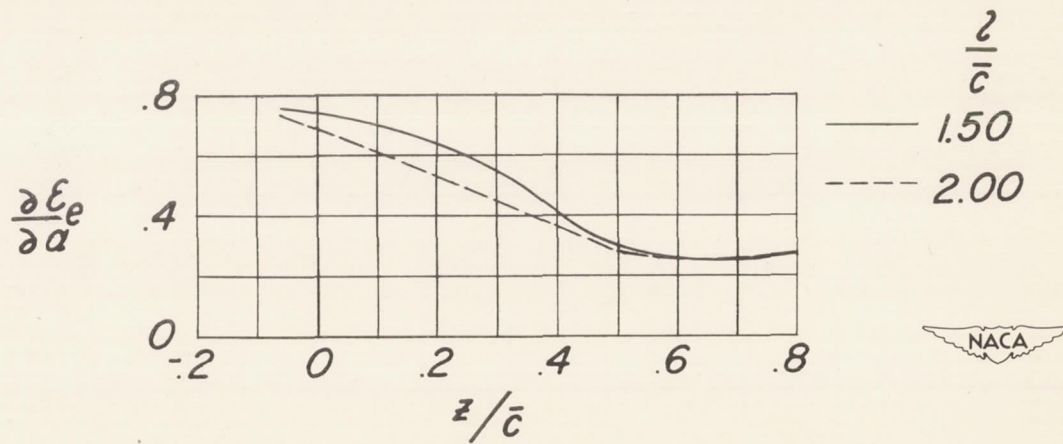
(b) $\partial\epsilon_e/\partial\alpha$ against $z/\bar{c}$.

Figure 36.- Variation of $\partial\epsilon_e/\partial\alpha$ with tail length and tail height.
H_2; $\alpha = 0^\circ$; $i_t = 0^\circ$.
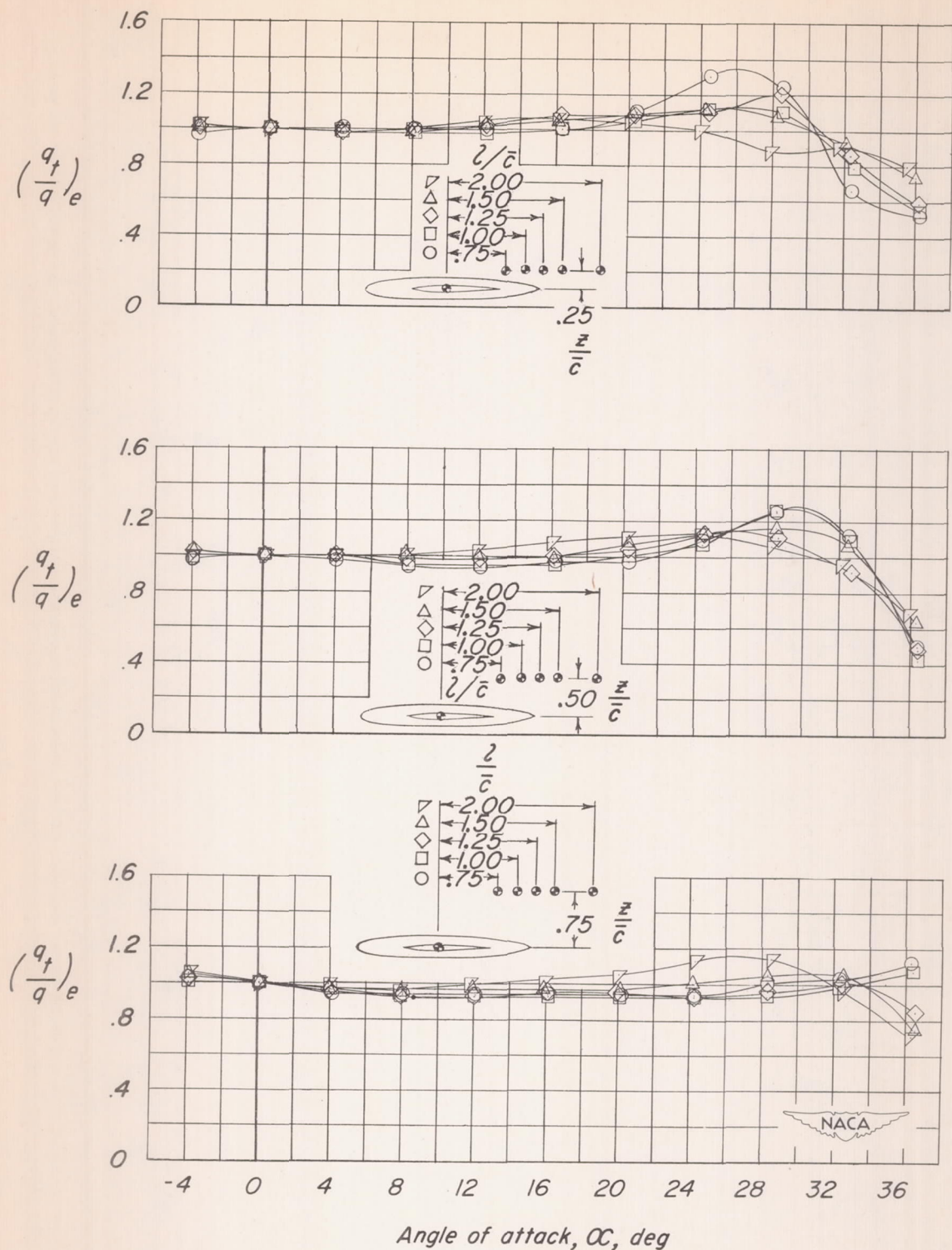
Figure 37.- Effect of tail length and tail height on variation of $(q_t/q)_e$ with angle of attack for a 60° triangular-wing model having a triangular all-movable tail. H_2; $i_t = 0^\circ$.
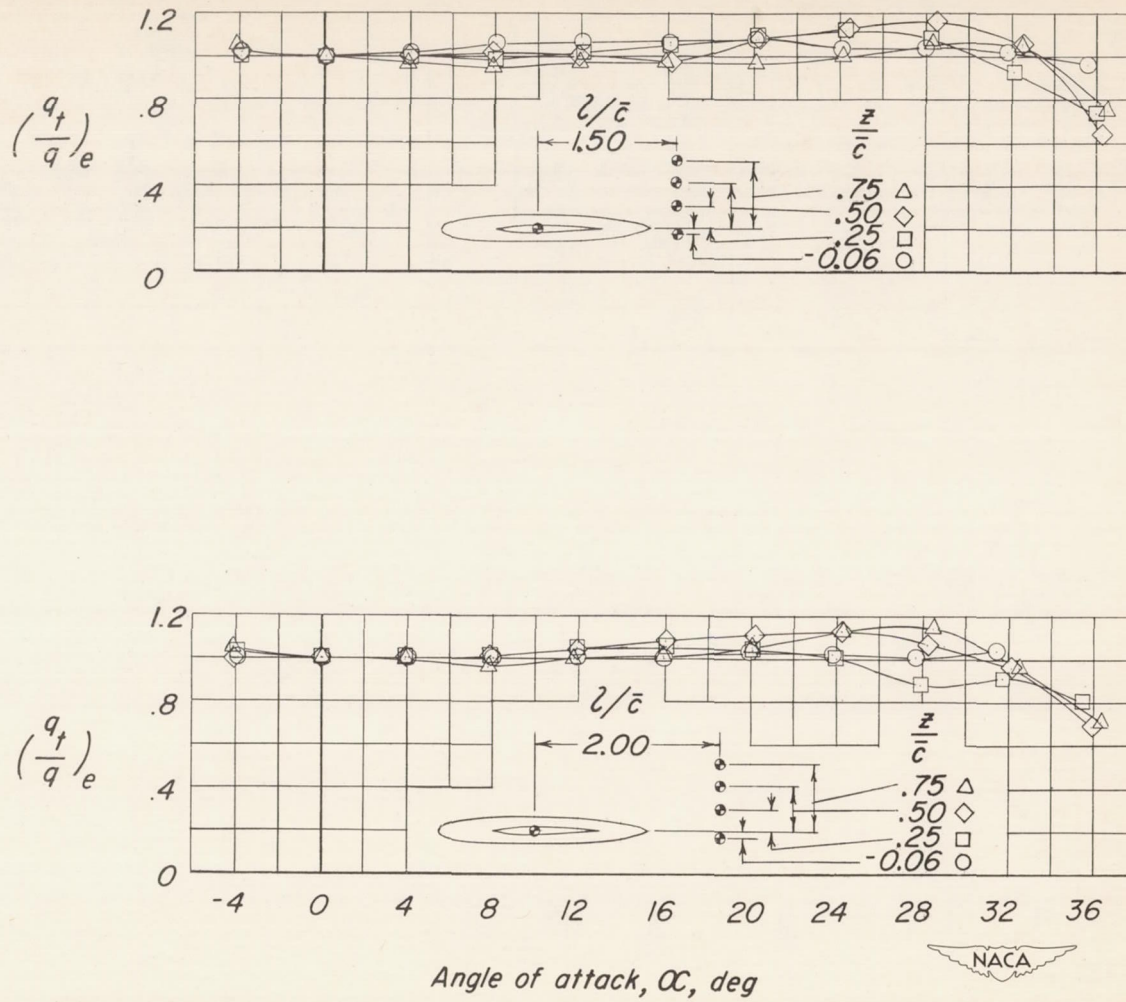
Figure 38.- Effect of tail height on variation of $(q_t/q)_e$ with angle of attack for a 60° triangular-wing model having a triangular all-movable tail. H_2; $i_t = 0°$.
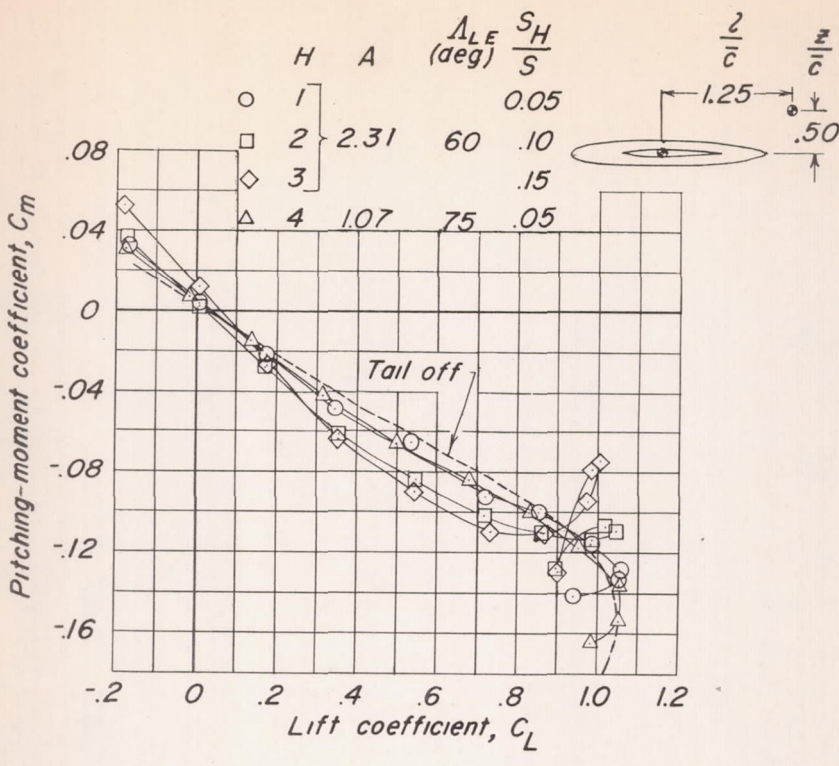
(a) $C_{m_{C_L}}$ varied.
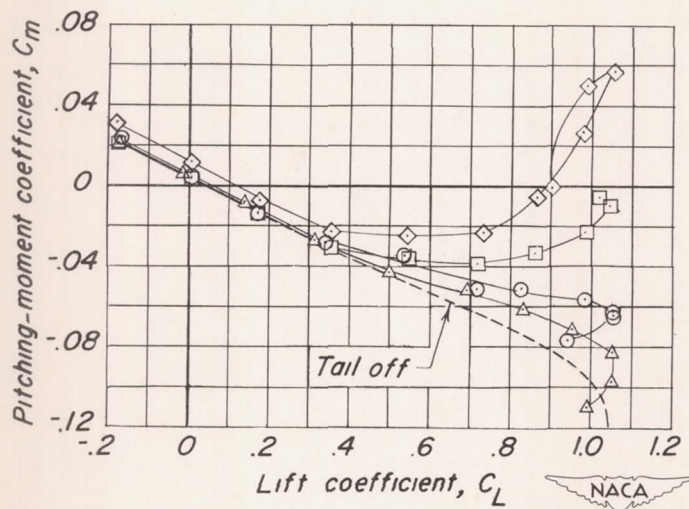
(b) $C_{m_{C_L}} = -0.10$.

Figure 39.- Effect of tail area and aspect ratio on static longitudinal stability characteristics of a 60° triangular-wing model having a triangular all-movable tail.
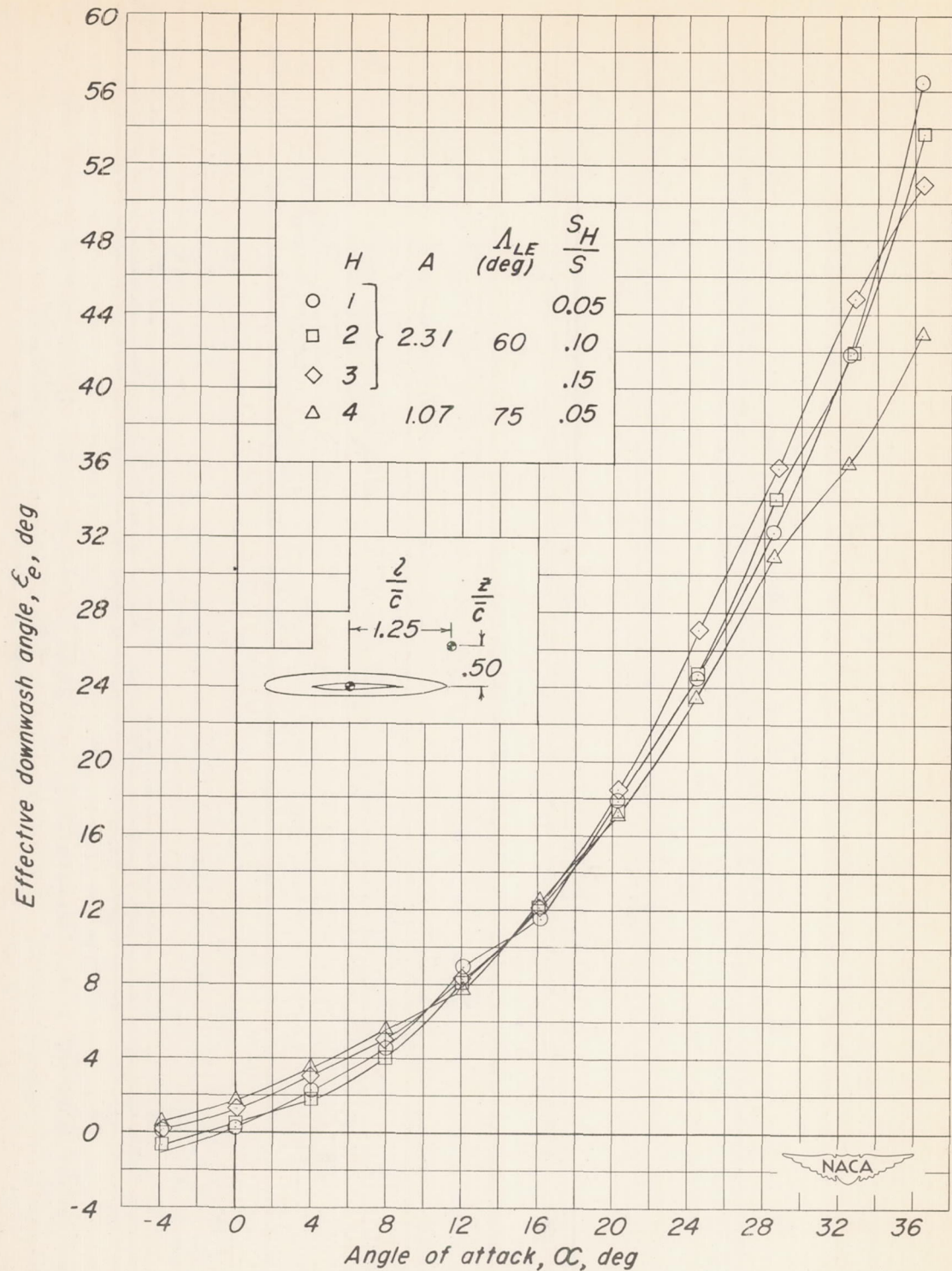
Figure 40.- Effect of tail area and aspect ratio on variation of effective
downwash angle with angle of attack for a 60° triangular-wing model
having a triangular all-movable tail.

	H	A	Λ_{LE} (deg)	$\frac{S_H}{S}$
○	1			0.05
□	2	2.31	60	.10
◇	3			.15
△	4	1.07	75	.05
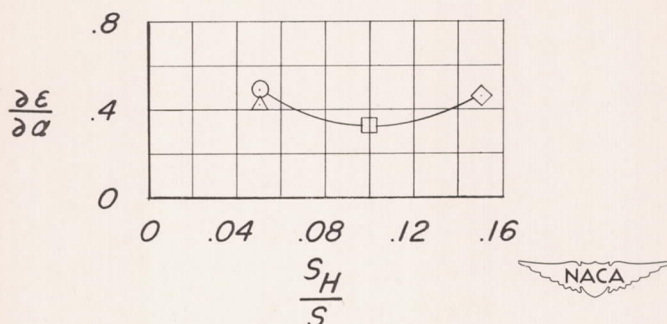
Figure 41.- Variation of $\partial\epsilon_e/\partial\alpha$ with S_H/S of a 60° triangular-wing model having a triangular all-movable control surface. $\alpha = 0°$.
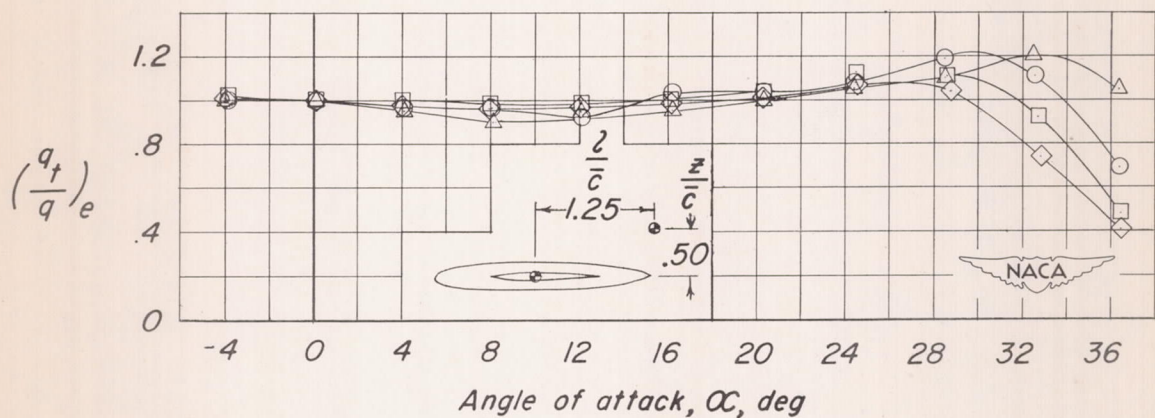
Figure 42.- Effect of tail area and aspect ratio on variation of $(q_t/q)_e$ with angle of attack for a 60° triangular-wing model having a triangular all-movable tail.
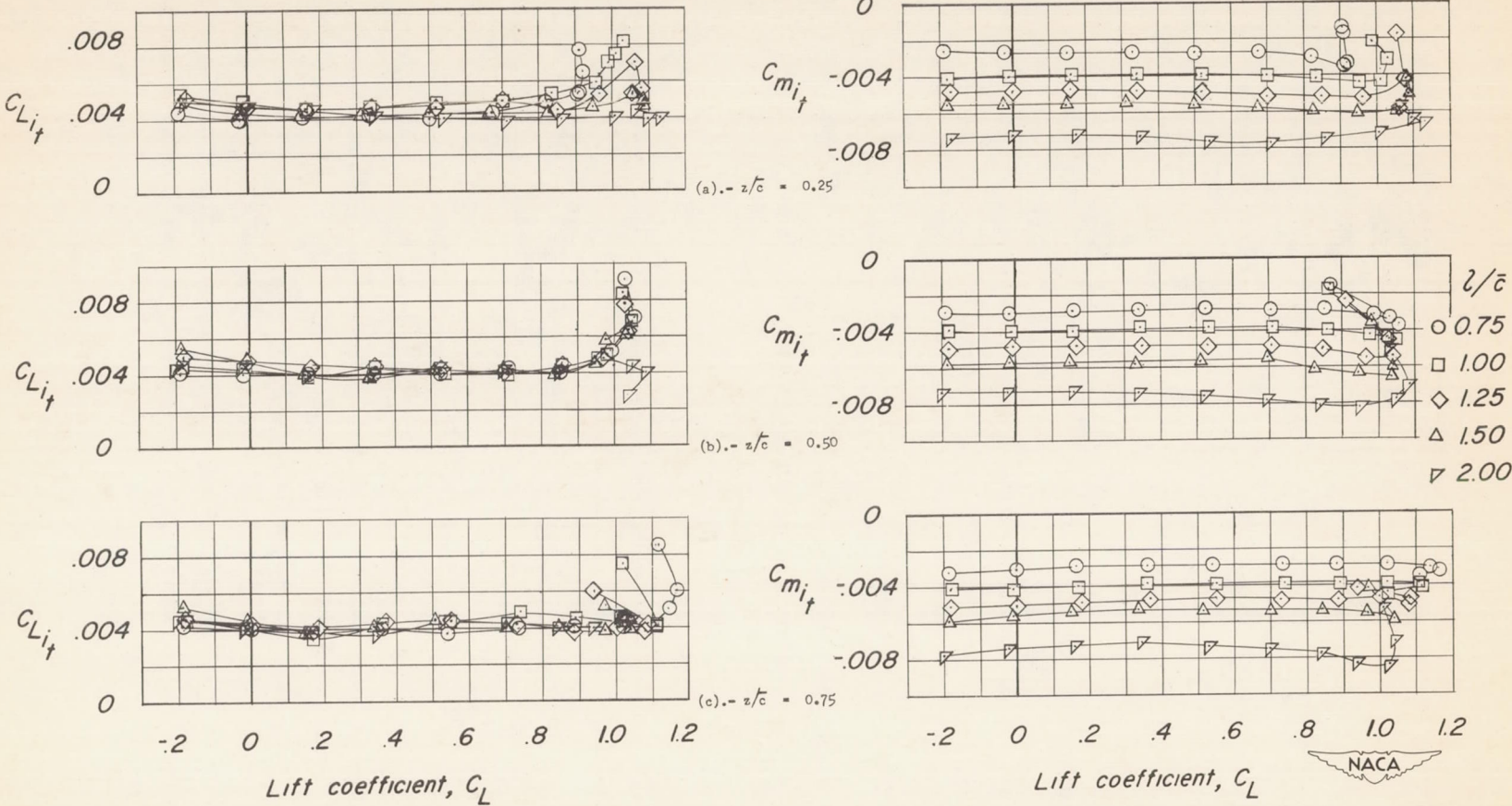
Figure 43.- Effect of tail length and tail height on variation of $C_{L_{i_t}}$ and $C_{m_{i_t}}$ with C_L for a $60°$ triangular-wing model having a triangular all-movable tail. H_2. $C_{m_{C_L}} = -0.10$ at $C_L = 0$. (See text for centers of gravity.)
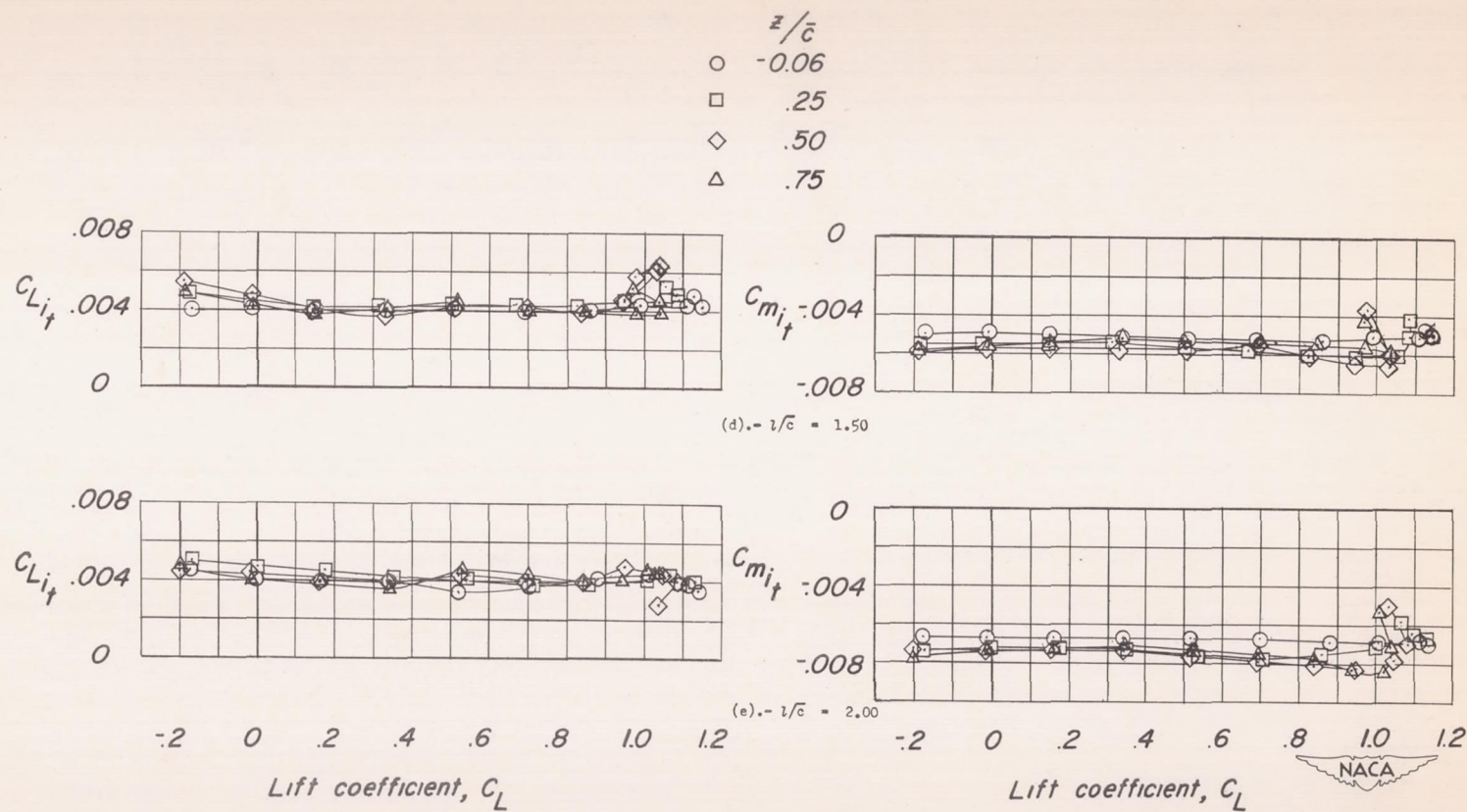
Figure 43.- Concluded.
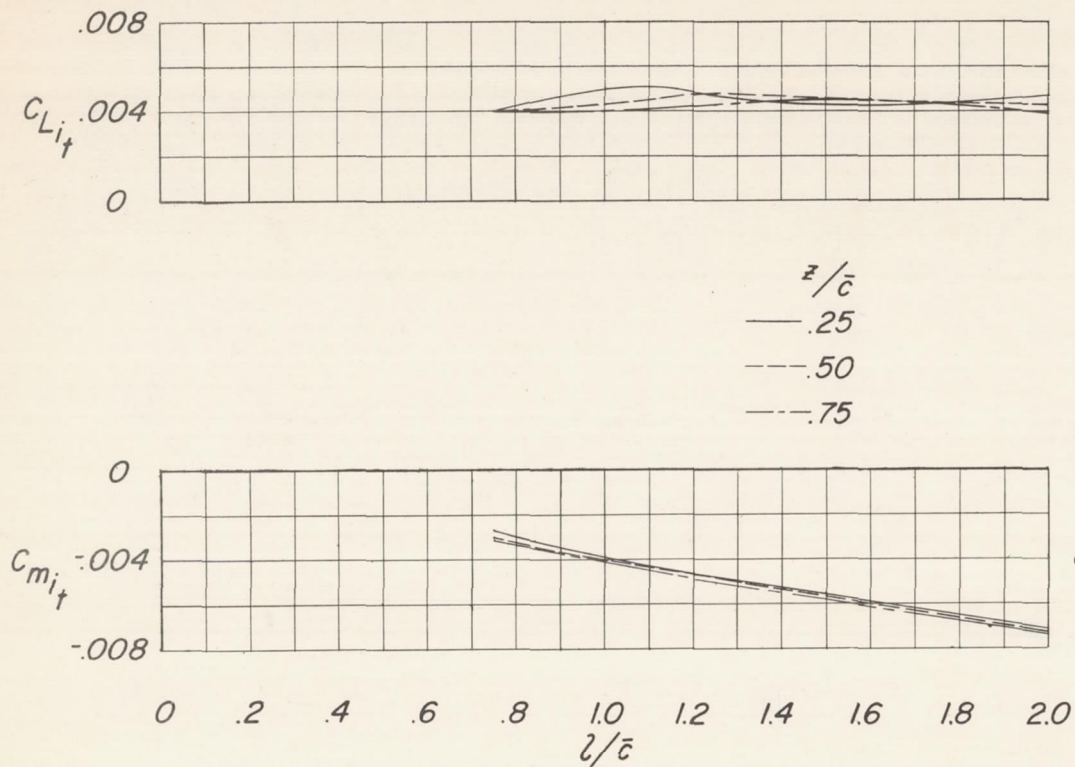
(a) $C_{L_{i_t}}$ and $C_{m_{i_t}}$ against $l/\bar{c}$. (b) $C_{L_{i_t}}$ and $C_{m_{i_t}}$ against $z/\bar{c}$.
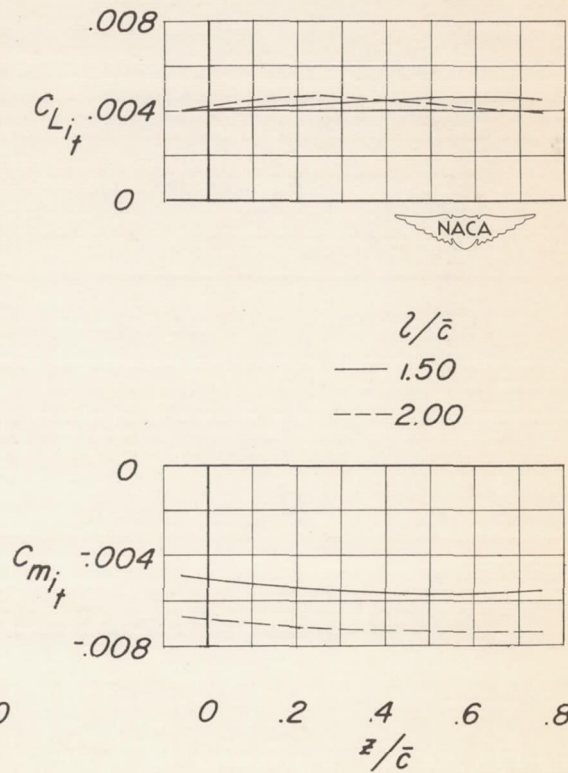
Figure 44.- Variation of $C_{L_{i_t}}$ and $C_{m_{i_t}}$ with tail length and tail height.

H_2; $C_L = 0$; $C_{m_{C_L}} = -0.10$. (See text for centers of gravity.)
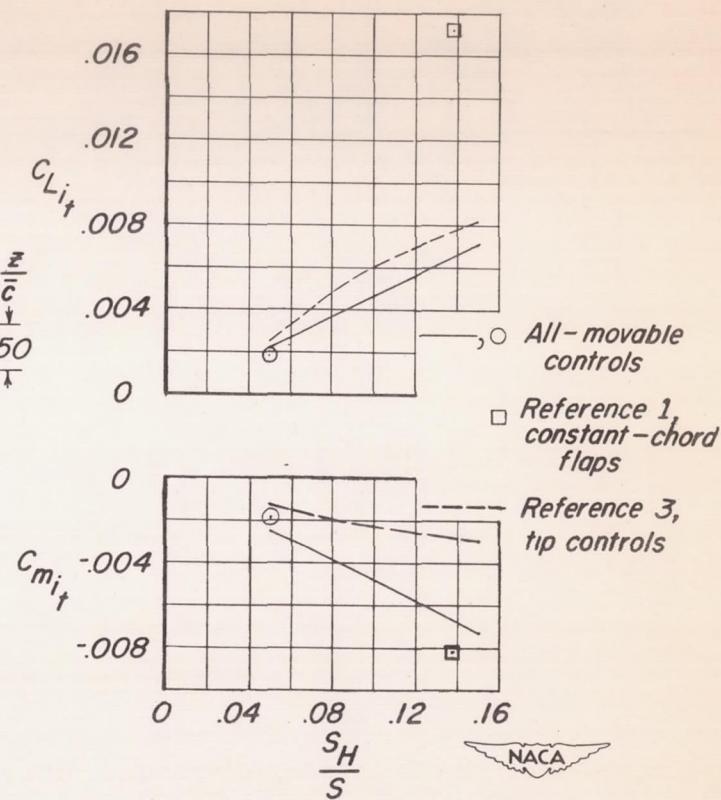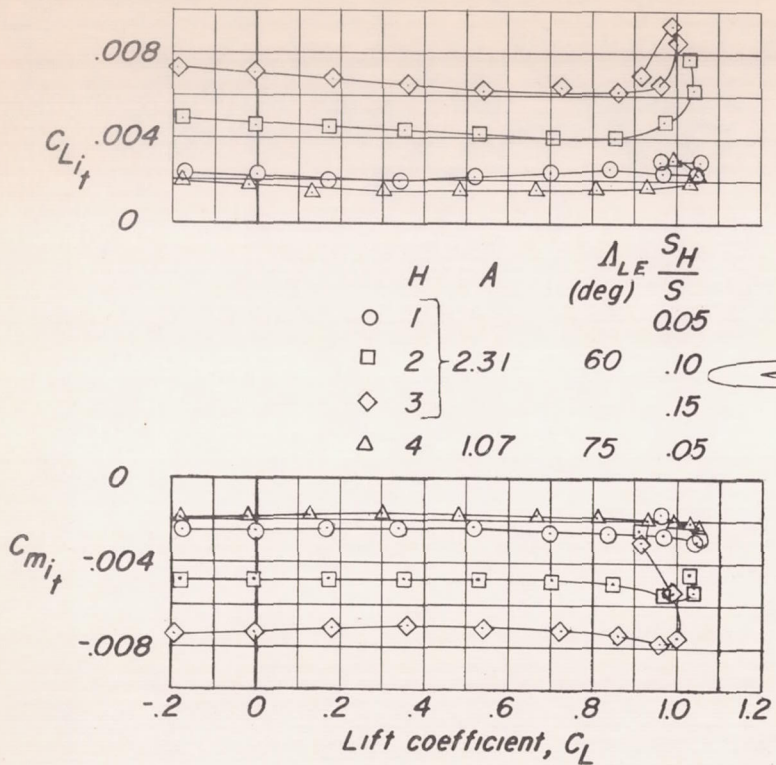
(a) $C_{L_{i_t}}$ and $C_{m_{i_t}}$ against C_L. (b) $C_{L_{i_t}}$ and $C_{m_{i_t}}$ against $\frac{S_H}{S}$ $C_L = 0$.

Figure 45.- Effect of control area and aspect ratio on $C_{L_{i_t}}$ and $C_{m_{i_t}}$ for

a $60°$ triangular-wing model having a triangular all-movable tail.
$C_{m_{C_L}} = -0.10$ at $C_L = 0$. (See text for centers of gravity.)